AN ABSTRACT OF THESIS OF

Brian M. King for the degree of Master of Science in Nuclear Engineering presented on June 12, 2012.

Title: Natural Circulation Scaling of a Pressurized Conduction Cooldown Event in the Upper Plenum of the Modular High Temperature Gas Reactor

Abstract approved:

_____

Brian G. Woods

In a Modular High Temperature Gas Reactor (MHGTR), the Pressurized Conduction Cooldown (PCC) event is an accident scenario in which there is a loss of forced convection of the coolant through the system but the pressure boundary remains intact. When the PCC event occurs, natural circulation onsets which results in a flow and temperature reversal, resulting in hot helium flowing into the upper plenum which could imping upon the upper plenum head. The High Temperature Test Facility (HTTF), which is being designed and constructed at Oregon State University, is a scaled thermal test facility of the MHTGR which is being built for both code validation purposes and to examine specific flow phenomena of the gas reactor. This study is being performed to determine how the HTTF simulates the same conditions as the MHTGR under this scenario through the use of scaling parameters and computational fluid dynamics.

Natural Circulation Scaling of a Pressurized Conduction Cooldown Event in the Upper Plenum of the Modular High Temperature Gas Reactor

by
Brian M. King

A THESIS
Submitted to
Oregon State University

in partial fulfillment of
the requirements for the
degree of

Master of Science

Presented June 12, 2012
Commencement June 2013

Master of Science thesis of Brian M. King presented on June 12, 2012.

APPROVED:

_____

Major Professor, representing Nuclear Engineering

_____

Head of the Department of Nuclear Engineering and Radiation Health Physics

_____

Dean of the Graduate School

I understand that my thesis will become part of the permanent collection of Oregon State University libraries. My signature below authorizes release of my thesis to any reader upon request.

_____

Brian M. King, Author

ACKNOWLEDGEMENTS

The author would like to express his appreciation to all those whose support he received during this process. Firstly, I would like to thank my advisor, Dr. Brian Woods, who has provided me with guidance and encouragement. He has always given me sound advice and assistance when I needed it and has made me well prepared for my future as an engineer.

I would like to thank Dr. Andrew Klein and Dr. Wade Marcum for always being willing to answer any questions I had during my work and providing their support when they could. I would also like to thank fellow graduate students Brian Jackson, Seth Cadell, and Aaron Weiss for their help and support.

I am very grateful to my grandfather, Frank Simon, for it is his encouragement that I have received my whole life that has led me to being an engineer, as well as the genetics that predisposed to me to be an engineer. I would also like to thank both of my parents who always believed that I would complete this task.

Finally, I would like to thank Ashley, who made it very clear that I better come home with my degree or not at all.

TABLE OF CONTENTS

TABLE OF CONTENTS (Continued)

LIST OF FIGURES

LIST OF FIGURES (Continued)

LIST OF TABLES

Natural Circulation Scaling of a Pressurized Conduction Cooldown Event in the Upper Plenum of the Modular High Temperature Gas Reactor

1 Introduction

The current generation of nuclear reactors in the United States includes 104 light water reactors (LWR), all of which rely on active safety systems which in turn rely on the performance and operation of pumps, electrical power, and can be affected by human performance. As power consumption grows, so does the need for nuclear power plants. The current proposed generation of reactors, the Gen III+ reactors such as the AP1000, are designed to advance the safety beyond that of the current generation of existing light water reactors through the implementation of passive safety systems. A passive safety system is designed so that natural physical forces such as gravity and pressure induce thermal hydraulic phenomena within the facility that result in a safe shutdown during accident scenarios without the use of safety systems that need to be actuated. The AP1000 is designed so that the in-containment refueling water storage tank has enough water for three days of operation following an accident, and once those three days pass, air cooling from natural circulation is sufficient (1).

Moving beyond Gen III+ is the GEN IV reactors. One of those proposed reactor concepts, the Very High Temperature Reactor (VHTR), is being designed to implement passive safety systems, such as intracore natural circulation for heat removal once an accident has occurred. The VHTR operates, as its name suggest at a high temperature, with an outlet temperature of 1000ºC which exceeds limitations of current material constraints. Due to material constraints, the High Temperature Gas Reactor (HTGR), which is similar in design to the VHTR but operates at a lower temperature, is the reactor with which this study is focused. Additional to the passive safety, the fuel of the General Atomics Modular High Temperature Gas Reactor (MHTGR) is designed in a way that allows for safe operation up to 1600 ºC. The HTGR is also designed such that its

components have inherently safe characteristics, such as the use of helium as a coolant, which operates in a single phase and is an inert gas.

1.1 Project Background

This study is part of work done at Oregon State University (OSU) in collaboration with the United States Nuclear Regulatory Commission (NRC), United States Department of Energy (DOE), and Idaho National Laboratory (INL) on the High Temperature Test Facility (HTTF). To accomplish the objectives of this project, a scaling analysis was performed on the Modular High Temperature Gas Reactor (MHTGR) which has informed the design of the HTTF.

The MHTGR is a prismatic HTGR design which uses helium as its coolant and graphite as its moderator. It is designed with a lower power density than LWRs allowing for safer operation at higher temperatures which leads to higher operating efficiency. Additionally, the safety is increased through the use of helium, which operates in single phase as an inert gas. Figure 1-1 shows a diagram of the GT-MHR which has the same overall design and is of a similar concept to the MTHGR.

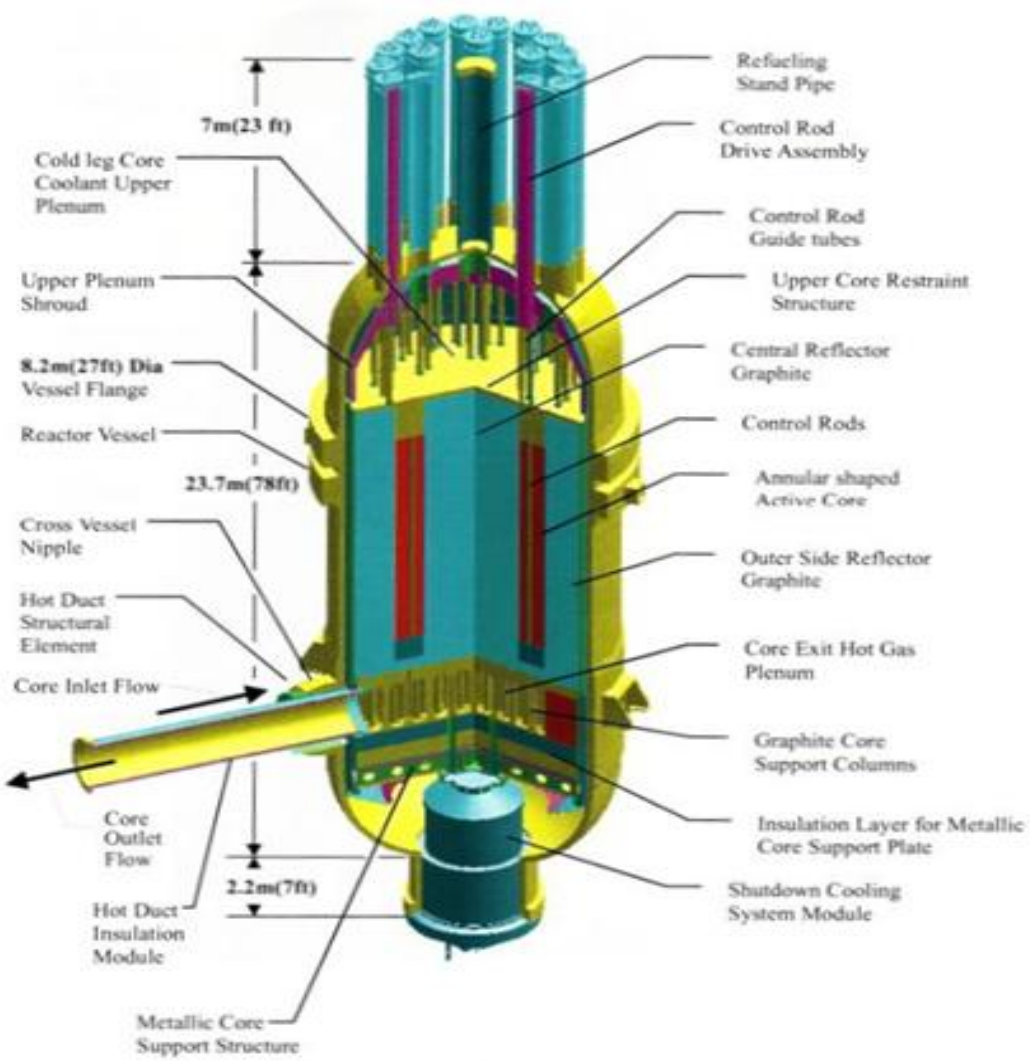

Figure 1-1: GT-MHR Diagram (2)

The HTTF is a thermal-fluid scaled integral test facility of the MHTGR. The primary purpose of the HTTF is to provide quality assured experimental data for code validation for various transient scenarios. In addition to this, the thermal fluid phenomena that occur during these transients can be examined. There are two main types of transients to be studied with the HTTF, the Depressurized Conduction Cooldown (DCC) event and the Pressurized Conduction Cooldown (PCC) event. A DCC event is an accident in which

there is a break in the pressure boundary of the system resulting in air ingress into the facility. A PCC event is an accident in which there is

no pressure boundary break, but a loss of forced convection occurs either from the shutdown of the circulator or from a break in the boundary between the inlet/outlet crossover duct which results in no break of the pressure boundary. A computer rendering of the HTTF vessel can be seen in Figure 1-2.

Figure 1-2: Oregon State University High Temperature Test Facility

The focus of this study is the inlet plenum, or upper plenum, flow mixing that occurs following a PCC event. Once a PCC event occurs, the decay heat in the core results in flow reversal and may result in the hot gas from the core entering into the upper plenum. The concern of this accident scenario is that once the gas flows into the upper plenum it could impinge upon the upper plenum doing damage to the reactor vessel resulting in a more serious accident.

There are two ways that the PCC event could occur, either through a complete loss of flow accident or from a break between the inlet and outlet duct.

In either case, it is postulated that once forced circulation is lost to the system, the buoyancy forces of the coolant fluid imparted by the decay heat in the core will be substantial enough to overcome the residual momentum and gravitational forces on the fluid resulting in flow reversal. There are several postulated flow patterns, which have been evaluated as part of this study. The one most expected in a loss of flow accident is one in which the hottest region of the core has the gas flowing upwards, and when the gas enters into the upper plenum it transfers heat to the upper plenum shroud and then flows down through the cooler regions of the core and where it then circulates back into the heated region. Because the MHTGR is designed with the heat sink at a lower elevation than the heat sink, intracore natural circulation is expected. When the intracore natural circulation occurs, it is expected that there will be only flow within the core and that no flow will pass down the upcomers.

It is important to understand the flow patterns that occur during this event. The flow patterns directly contribute to the passive safety of the reactor through their effect on the heat transfer. The natural circulation of the gas reduces the internal temperature of the core and transfers heat to the outer region of the core which then conducts through the core barrel and radiates off the surface of the vessel to the reactor cavity cooling system. This study is not being done to look at the effect that the circulation of the helium gas has

on the heat transfer, but how the gas flows in the upper plenum given the boundary conditions of the PCC event.

1.2 Research Objectives

The objective of this study is to determine the conditions of the PCC event in the HTTF and how they compare to that of those same conditions in the MHTGR. Due to the nature of scaling, it will be not be possible to achieve similarity in all aspects of the PCC event between the two facilities. Because of this, distortions will exist and this study can be used to characterize those distortions as the development of both the HTTF and MHTGR moves forward.

what conditions would be required to accurately model upper plenum mixing during the PCC event in the HTTF with respect to the MHTGR. This work was completed in two parts: (1) analytical scaling analysis of the PCC event and (2) computational fluid dynamics modeling of the PCC event for both the MHTGR and HTTF in StarCCM+.

The analytical scaling analysis was done by evaluating a non-dimensional momentum equation defined for mixing in the upper plenum. From this equation, three non-dimensional parameters were identified that characterize the upper plenum mixing: the Froude number, the Reynolds number, and the ratio of inlet plenum length to flow channel diameter. This analysis looked at maintaining the similarity between model and prototype through the use of non-dimensional parameters through three methods: (1) temperature scaling, (2) forced convection of coolant in HTTF, and (3) using nitrogen instead of helium in the HTTF analysis. This part of the analysis also looked at determining what the natural circulation velocity of the coolant is once flow reversal has happened. The natural circulation velocity is the velocity that is present in both the Froude and Reynolds equations. This was done through the evaluation of a loop momentum balance equation. Through the use of the three methods used for scaling, a series of values for the non-dimensional parameters in both facilities were determined, along with the relative distortion of each method. These results are used as the input for the CFD modeling. This work and its corresponding results can be found in Chapter 4.

The computational fluid dynamics modeling of PCC mixing in the upper plenum was done by creating and running models of both the MHTGR and HTTF. A series of different models for the PCC event in the upper plenum were created. It is expected that during the PCC event, some of the outer flow channels will operate in downflow while the inner channels will be in upflow.

A sensitivity study was performed by running three types of models for a range of upflow to downflow ratios: (1) 25% of channels in upflow, 75% of channels in downflow, (2) 50% of channels in upflow and 50% of channels in downflow and (3) 100% in upflow and upcomer inlet set as an outlet., The breakdown of what simulations were run can be found in Chapter 5, while the results of the three models for the MHTGR and six models for the HTTF can be found in Chapter 6.

1.3 Assumptions and Limitations

1.3.1 Assumptions

This study was done assuming that loss of flow has occurred and that flow reversal and intracore natural circulation have onset. This means that instead of the helium gas flowing down through the core, there will be upflow in some of the flow channels resulting in gas jets entering the upper plenum. If the jets stay intact they could impinge upon the upper plenum ultimately doing damage to the system. There is also the possibility that the jets will diffuse into bulk flow and will not impinge upon the upper plenum. Once the jets either lose their momentum or hit the upper plenum, they will transfer heat to the upper part of the vessel and move to the outer radial region of the upper plenum and fall back into the outer regions core.

1.3.2 Limitations

This study consists of analytical scaling that is used to define a series of flow models which were built in Star-CCM+ to determine how well the HTTF can be used to scale the upper plenum mixing during the PCC event through the use of comparisons between

models for both the HTTF and MHTGR. No experimental data has been taken as part of this study. The scaling work that has been done is only applicable to this scenario and not to the facility as a whole. The overall scaling parameters such as temperature, pressure and power scaling as well as the choice of gas may be varied from that of standard operations for the HTTF, but only with respect to this analysis. The geometric parameters of the facility such as core length, upper plenum height, and flow channel diameter are constraints and cannot be changed for this analysis.

1.4 Outline

This chapter describes the background for this study. This includes the background of the HTTF project and its relevance with respect to the MHTGR. Additionally, this chapter states the objectives and importance of this thesis study.

Chapter 2 provides information on the work done in this study, including: natural circulation/convection in nuclear reactors from both analytical and numerical perspectives, buoyancy driven flow reversal, pressurized conduction cooldown events, pressurized loss of forced convection events, and jet impingement. An explanation and background of how Star-CCM+ was applied in this work with respect to the models that were used and how they work is also included in this section.

Chapter 3 provides a description of the facilities associated with this study including the MHTGR and the HTTF. It also describes the previous scaling work and how it is used in this study.

Chapter 4 presents the analytical work completed for this study by the author that bridges the gap between the previous scaling work and the study, as well as the work that has been done to set up the information needed for the models.

Chapter 5 presents the Star-CCM+ models utilized as part of this work including a simplified model of the system to establish boundary conditions and basic flow patterns and that primarily describes the work. Also in this section, is a model of the MHTGR under similar conditions for validation on the ability for the HTTF to model the PCC.

Chapter 6 presents the results of the models and what significance they actually have to the work.

Chapter 7 presents the conclusions from this work and any future work that needs to be done.

2 Literature Review

This section discusses the literature review that was done as part of this overall work with the following categories: natural circulation/convection, buoyancy driven flow reversal pressurized conduction cooldown, pressurized loss of forced convection, scaling, effects of other gases, gas jet impingement, and CFD modeling.

2.1 High Temperature Gas Reactors

There are many different types of high temperature gas reactors that will be discussed throughout this literature review so it is important to understand each of them and how they are both similar and different to the MHTGR, which is the focus of this project.

The MHTGR is the third generation of gas cooled reactors (3). The idea behind them is that through the use of tiny fuel particles coated with porous graphite and then covered by layers of pyrolytic carbon, silicon and carbide, the particles would be robust enough to stand up to large temperature transients and would not fail below 1600 ºC. Four other reactor types of gas reactors are discussed throughout this literature review: Gas-Turbine-Modular Helium Reactor (GT-MHR), High-Temperature Thermal Gas-Cooled Reactor 10 (HTR-10), High Temperature Test Reactor (HTTR), and the Gas-Cooled Fast Reactors (GCFR) (4).

The GT-MHR is a 600 MW prismatic helium-cooled graphite-moderated reactor developed by General Atomics that was originally designed to operate using plutonium to aid in the reduction of Russian weapons grade plutonium. It maintains many of the same overall design safety features as the MHTGR including use of inert fluid as a coolant, graphite core for slow thermal response and stability at high temperatures, and a lower power density core with a steel reactor vessel surrounded by a reactor cavity cooling system which allows for passive cooling to keeping the temperature below design limits. (5)

The 10 MW High Temperature Gas-cooled reactor (HTR-10) is a pebble bed graphite-moderated helium gas-cooled reactor with 10 MW thermal power and an outlet temperature of 700ºC and an operating pressure of 2.5 MPa. Two safety demonstrations were performed on the HTR-10 to demonstrate inherent safety features as well as to obtain transient data for safety analysis codes. Both of these demonstrations were anticipated transients without scram (ATWS) tests. The test of specific interest to this study is the shutdown of the helium circulator which resulted in a decrease in the reactor core power and an increase in the upper reflector temperature as well as the upper part of the side reflector but a decrease in temperature of other parts of the core structure. (6)

The HTTR is a 30 MW helium-cooled graphite-moderated prismatic high temperature gas reactor designed to obtain characteristic data for HTGR's (7). Similar to the HTTF, the HTTR is designed primarily for the evaluation of depressurized events as they are the more severe accidents postulated for the high temperature gas reactors. (8) (9)

The GCFR is helium cooled fast reactor. Because it does not have the graphite core that the other gas reactors do, it is not able to maintain reactor stability during an accident scenario through passive safety alone. (4) (10)

The main similarity between these four reactors is that they have the same expected flow paths during pressurized or depressurized accident scenarios.

2.2 Natural Circulation/Convection Studies

Passive safety heat removal was evaluated for a GCFR design, was evaluated by Cheng (4) was based on that of the high-temperature thermal gas-cooled reactors (HTRs). In this reactor design, natural convection coupled with in-vessel emergency heat exchanger as well as a hybrid active/passive safety system is utilized for post-accident cooldown. The need for a partially active system comes from the GCFR having too high of a power density for purely passive cooling to be effective. It was found that passive safety alone, for low pressure cases, was insufficient to keep the system below its maximum

temperature limit. From this, it can be summarized that power density and pressurization directly affect the capabilities of natural convection passive cooling.

Celata (11) studied upflow conditions of forced and mixed convection in water cooled vertical pipes, where natural convection has a significant impact on forced convective flow through a buoyancy driven force. In this evaluation the buoyancy forces were represented by the Rayleigh number with the pressure gradient forces represented by the Reynolds number for buoyancy forces and the opposite for forced flow. An experimental apparatus was constructed with a three-head piston pump system to analyze this problem. The further into mixed convection zone of flow the system reached, the higher the errors there were found to be in calculating the heat transfer coefficient. This analysis has shown that the low-Reynolds k-ε for developing flow in a tube shows close agreement with the mixed convection flow in vertical pipes; however, its influence on the heat transfer in mixed convection for both the aided and opposed mixed convection cases shows that it is not useful for practical purposes and would be more reasonable to look at other ways to determine the heat transfer coefficient under these conditions. From this a new method for determining the heat transfer coefficient in upward mixed convection flow in a vertical channel was determined with similarities to other methods. It was determined that as L/D increases, the heat transfer decreases with a maximum decrease achieved when the buoyancy parameters reach a point of unity.

Mohammed (12) discussed the importance of mixed convection in the laminar flow regime with respect to convective heat transfer is discussed. This problem was evaluated experimentally in a heated tube with air, as the working fluid, circulated by a centrifugal fan. A series of test runs were carried out over various laminar Reynolds number ranges and various Grashof ranges for assisted and opposed flows. Relevant conclusions from this work included that at a high Grashof number and low Reynolds number, it was found that in the heated section fully-developed flow was not achieved due to the presence of flow reversal, with a lower the Reynolds number, the higher the surface number, and the

surface temperature variation was found to be a function of both Reynolds and Grashof numbers.

2.3 Buoyancy Driven Flow Reversal

The paper by Sabwarhall (13) discusses CFD analysis for natural circulation in a GCFR. For the first 24 hours, plume behavior is not considered as the forced convection required from the blower prevents recirculation. Plume behavior is soon once natural circulation and flow reversal onset and is attributed to the reduction in mass flow rate. The CFD analysis was run using Fluent with inputs form GAMBIT and RELAP5. The goal of this work was to understand the interaction of hot plumes in the upper plenum. The flow channels for the core were modeled as the upper plenum inlets and the gap between the reflector and the shield, emergency core cooling system and the power conversion units were used as the outlets. A series of trials were run changing the location and changing what inlets and outlets were open. The key thing to take away from this study is that the flow path follows that of the temperature profile. As the temperature decreases so does the flow rate, and where no temperature gradient is found little flow is found. Additionally, while it was determine that the net mass flow rate was taken to be positive; the mass accumulated into the upper plenum was determined to be negligible allowing for the problem to be modeled as steady state.

Cheng (14) evaluated the effects and development of buoyancy-assisted flow reversal in vertical circular channels. Buoyancy assisted flow reversal phenomenon was determined to be a profound influence on flow instability and thus heat transfer. This study looked at the problem with a heated slab with circular channels where the temperature was not uniform throughout the slab. It was seen that the “fluid near the hotter side is accelerated due to the buoyancy” and thus reversed flow is seen near the cold area. This occurs corresponding to the ratio of Reynolds number to Grashof number. As the ratio decreases, the strength and amount of flow reversal increases. Within a single pipe, where

there are regions of up and down flow, a series of rings develop such that at the center of each side the highest velocity occurs and it decreases the closer to the outside of the pipe and to the other region such as if it were a boundary.

2.4 Pressurized Conduction Cooldown/Loss of Forced Convection

The paper by Haque (15) presents numerical simulations of the VHTR using THERMIX to look at both PCC and DCC conditions. This study looked data from the CRP-3 benchmark problem for the GT-MHR. Both depressurized and pressurized conduction cooldown were evaluated. For the pressurized case, a system pressure of 55 bar was assumed following SCRAM, with heat transfer from conduction and radiation caused by natural convection. At high pressure, helium natural circulation occurs in core as well as in the top and bottom reflectors.

The temperature distribution over time during pressurized cooldown can be seen in Figure 2-1.

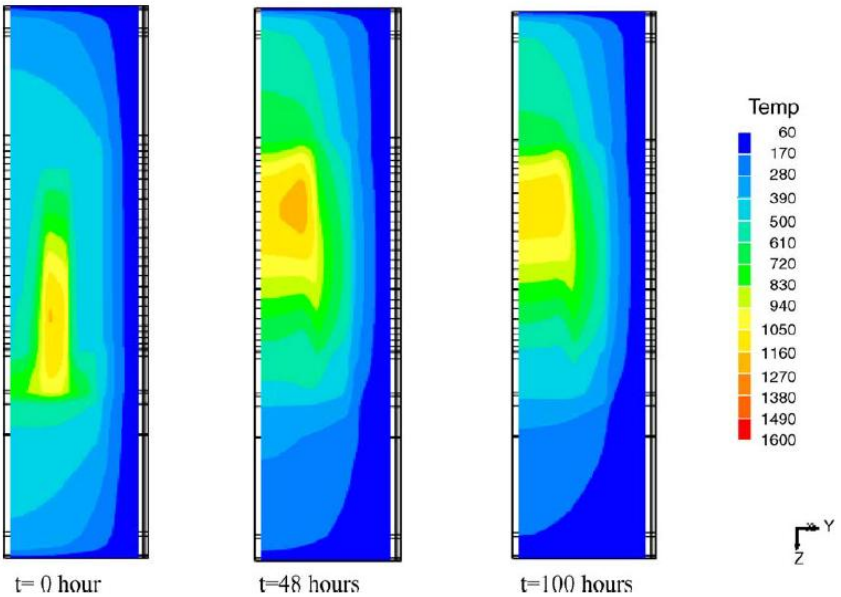

Figure 2-1: VHTR Pressurized Cooldown Temperature Distribution (15)

Initially at 0 hours, which would be the conditions under normal operations, the helium gas jets flow from the upper plenum down through the core. This results in the coldest temperatures being at the top of the core, with the gas increasing in temperature the further it travels through the core. Once the forced convection ends and the accident scenario begin, the buoyancy forces of the fluid imparted by the decay heat in the core begin to overcome the gravitational forces and remaining inertia of the fluid. Once natural circulation begins and the coolant begins flowing up through the core the temperature reverses. After 100 hours of this, the temperature profile settles on what is seen on the right side, where the hottest part of the core is now just below the upper plenum.

The flow patterns that correspond to the temperature distributions in Figure 2-1 can be seen in Figure 2-2 where the hotter regions of the core have upflow and the colder regions have downflow.

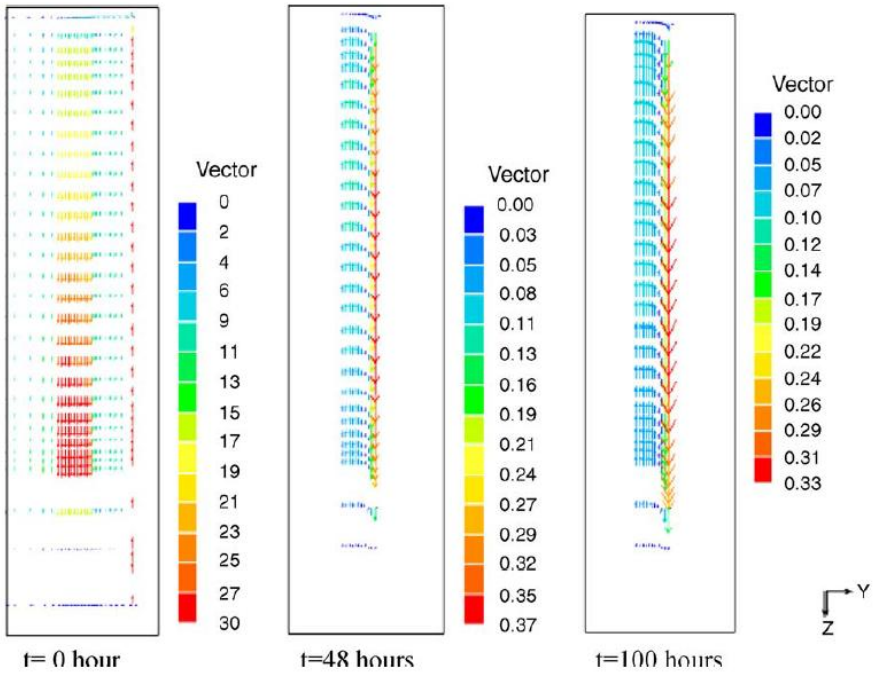

Figure 2-2: VHTR Gas Velocity Vectors During Pressurized Cooldown (15)

During normal operation, which is what's seen in the 0 hour part of the figure, the coolant flows down through the core from the upper plenum via forced convection. Once the accident scenario has progressed, and natural circulation onsets, what is seen in the other two parts of the figure occurs, where the central heated gas channels are in upflow with the outer cooler channels in downflow.

Over time the velocity appears to stabilize eventually resulting in a steady state flow reversal and a velocity gradient that is related to temperature profile. Additionally, the radial and axial temperature profiles can be seen in Figure 2-3.

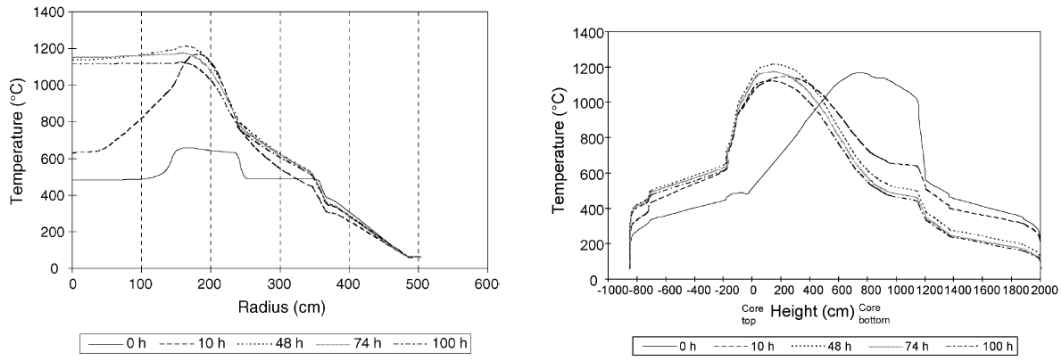

Figure 2-3: Temperature Distribution at Maximum Temperature Location (15)

In Figure 2-3 the temperature profiles for axial and radial temperature profiles are shown where there difference between normal operations and PCC temperature profiles can be seen. The temperature reversal can be seen in the second part of the figure, where the top of the core is seen as the highest temperature very quickly once the PCC even has begun.

A very important point can be taken from these graphs and this work: once the accident begins the temperature profile of the system changes eventually resulting in flow reversal and a temperature reversal. A similar effect was seen by Chen (16), although because the reactor was the lower power HTR-10, the the time that it took for these thermal phenomena was significantly shorter than what was seen in the GT-MHR case. Additionally, the occurrence of the hotter temperatures in the upper regions of gas

reactors during a pressurized loss of forced convection (P-LOFC) is something that was also identified by the IAEA (17).

Dunn (18) looked at the effect of various MHTGR designs with varying powers, number of fuel columns, power density and vessel inside diameter, but with the same pressures and inlet and outlet temperatures. The powers range from 410 MWt to 500 MWt, with the power density of 63W/cm^3 corresponding to the 410 MWt case and 62W/cm^3 corresponding to the 500 MWt case. The temperature of the upper plenum shroud was found to range between 735ºC to 771ºC, which is under the 815ºC maximum allowed temperature. From the data, the lowest power core design, which had the highest power density had the highest upper plenum shroud temperature. Only the highest power case was found to have equal upper plenum shroud temperature. What should be noted from this is that even for the worst case design, the temperature remains under the maximum allowed temperature. The decay heat for this study was set to 12%, with 2% accounting for power level instrumentation uncertainty and the other 10% accounted for uncertainty in actual decay heat, material properties and method of calculation.

In their paper, Kunitomi et al. (19) define a pressurized accident as one that is caused by a break internal to the system that does not result in depressurization which is equivalent to an inlet/outlet crossover duct. The work was done based on the HTTR. The thermal hydraulics code TAC-NC was used to analyze temperature transients during both the depressurized and pressurized cases. In the pressurized case it is shown that helium flows up through the reactor core and downwards along the reactor pressure vessel inner surface through the mode of natural circulation which transfers the cores decay heat the pressure vessel which then loses heat vessel cooling system through radiation and conduction of air, where radiation is the dominant method. A maximum temperature is reached after 10 minutes in the pressurized condition at just under 400 degrees ºC above that of the core outlet temperature. Under this condition, the maximum temperature occurs in the upper part of the core because the natural circulation transfers the decay

heat to that region. With proper insulation, the top head of the pressure vessel remains well under the core inlet temperature. Additionally after a 30 hour time period has passed, natural circulation provides less than one-fifth the heat removal rate that conduction through the core structure provides. Part of the reason for this is that heat transferred through natural circulation is transferred to the graphite blocks in the upper core region. Based on their design, as long as the system remains pressurized, if the vessel cooling system fails, the reactor pressure vessel would not reach a temperature that is significantly higher than that seen when the coolant is active. The heat transfer through the graphite being the primary source of decay heat removal as compared to the natural circulation of the gas was also seen in HTR-10 analysis done by Wu (20).

In the paper by Ball (21) accident scenario simulation results for both the prismatic and pebble bed core HTGR variants sensitivity studies are looked at to help quantify uncertainties using an Oak Ridge National Laboratory Graphite Reactor Severe Accident Code (GRSAC) (22) are presented. The accidents evaluated includetwo types of loss of forced circulation accidents, pressurized and depressurized (D-LOFC). The start of a LOFC run was run from operating conditions to a LOFC with a flow coastdown transient. For the P-LOFC case, a passive reactor cavity cooling system was considered to be operational, which results in the core temperatures being fairly uniform and results in lower peak temperatures than the depressurized case due to the buoyancy flows. This also results in higher temperatures near the top of the core and a maximum fuel temperature of just below 1300 °C after 24 hours and eventually reducing to just above 1000 °C by 120 hours. The study also suggests that the driving controller of the success of the outcome of the P-LOFC is the emissivity for the radiation between the vessel and the RCCS and that the effects on the system are not nearly as severe as they are for the D-LOFC event but the reactors should be able to withstand both events.

2.5 Scaling

In the paper by Zuber (23), the development of the methodology of scaling that was used in the work that this study is built on is discussed. The methodology was developed as an important element of the US NRC Severe Accident Scaling Methodology development program. It employs a hierarchical, two tiered scaling analysis, starting with system decomposition which provides system hierarchy and identifies geometric processes and then moving into a second part which includes scale identification and looks at volumetric, area and time scaling. The third level of this approach is top-down or system scaling analysis and the fourth and final level is bottom up process scaling analysis. The top down and bottom up processes are combined to provide the two tiered analysis which is designed to handle five objectives: 1) "provides a methodology that is comprehensive, systematic, auditable and traceable", 2) "provides a scaling rationale and similarity criteria", 3) "provides guidelines for reviewing facility design and test conditions", 4) "ensures prototypicality of experimental data for important processes", and 5) "quantifies effects of distortion".

This overall methodology can be seen in the flow chart below Figure 2-4.

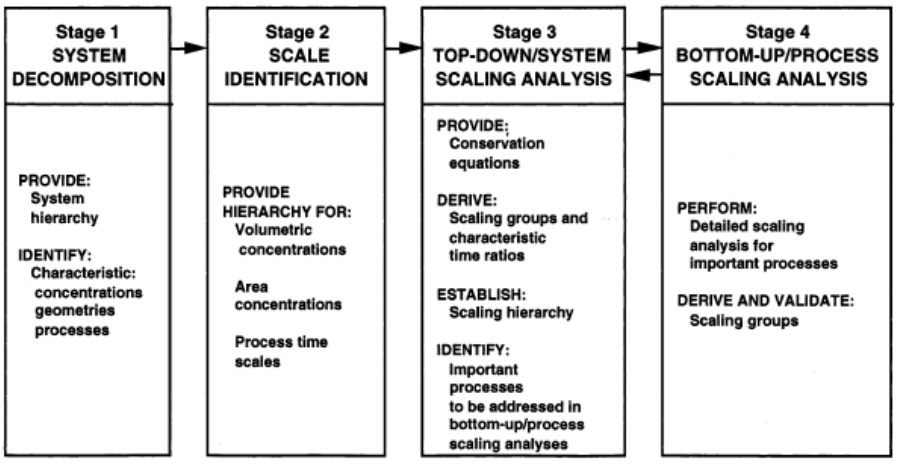

Figure 2-4: Flow Diagram for Two-Tiered Scaling Analysis (23)

The two-tiered scaling methodology was used in the development of the work done by Reyes (24), which was the basis for much of the work that was used to develop the HTTF and the scaling analysis that was completed to support this work.

Ishii's (25) paper discussed the development of the Purdue University Multi-Dimensional Integral Test Assembly (PUMA), a scaled test facility of the simplified boiling water reactor, which used a similar methodology as the Zuber two tiered methodology. The relationship between reduction of cross-sectional area between a scaled facility and a prototypical facility which results in an increase in surface-to-volume ratio was identified as an area that causes distortion because of the effect on heat transfer area. One of the main conclusions of importance from this study is that all the scaling requirements cannot be satisfied and that "some scale distortions are inevitable". Two reasons for distortion were identified: "difficulty in matching the local scaling criteria and lack of understanding of a local phenomenon itself". This results in great difficulty to directly use results from a scale facility to represent a prototypical facility, but can be mitigated by characterizing the distortion.

2.6 Effects of Other Gases

In his paper Epiney (26) looked at the effect of injecting heavier gases into the reactor system under depressurized conditions. It discusses the issue with decay heat removal that gas cooled fast reactors have due to their high core power density. The heavier gases being considered for injection are nitrogen and CO_2. The reference reactor design for this study is designed to prevent depressurization below one MPa, which is the limit for the blower power. This system actuates whenever the vessel pressure drops below 3 MPa. The initial injection into the system of the heavier gas is limited by the upstream pressure. No concern is shown for oxidation because previous studies show this only occurs above 1600ºC. The importance of this study to my overall work is how different gases react under similar conditions. Their ability to cool was defined by the product of their density and specific heat as well as their mass flow rate, and it was shown that the cooling

capabilities of helium are far insignificant to that of other gases, and this is primarily because of its much lower density.

2.7 Gas Jet Impingement

The effects of a jet impinging on a spherical cavity was looked at in Terkhov's (27) paper. The experimental set up was from a subsonic nozzle with a low turbulence ($Re \sim 10^4$) onto a spherical cavity. Three regions are seen, where the flow impinges directly on the wall, where the jets turn upon contacting the wall and form vortices, and an annular region with a laminar boundary layer. Instead of turning at a 90 degree angle as the flow does when it hits a flat surface it was seen that the flow entering the cavity reflected back out of the cavity at 180 degrees opposite to where it entered, resulting in flow pulsations. The important thing that can be taken away from this study is that the rate of heat transfer to the cavity surface was less than the rate of heat transfer to a flat surface and is largely dependent on the relationship between the nozzle diameter and the cavity diameter.

2.8 CFD Modeling

In the paper by Yoo (28), CFD-assisted scaling was discussed which pertains directly to the work done in this study. In this case the study focuses on the use of Fluent for heat transfer in PWR spent fuel pools. The goal was to determine the peak cladding temperature using a scaled down single fuel assembly. The scaling parameter and initial conditions of the CFD model were the first things developed. It was determined that although thermal similarity could be set for the facility, flow similarity could not be preserved due to facility complexity. In the development of the CFD model, it was determined that a one-eighth slice of the entire geometry was adequate to fully represent the phenomena expected. The conclusion of this study showed that while temperature similarity was conserved, the other thermal hydraulic parameters, while not preserved, did not pose an issue to the requirements for the scaling and study in the case.

3 Facility Descriptions

This section provides a more detailed description of the two facilities of interest in this work, the MHTGR and HTTF.

3.1 Modular High Temperature Gas Reactor

3.1.1 MHTGR Operation Characteristics

The MHTGR is a prismatic helium cooled, graphite moderated 350 MWt high temperature gas reactor (28). In Figure 3-1 is shown the GT-MHR, which, while different from the MHTGR, has the same basic overall design.

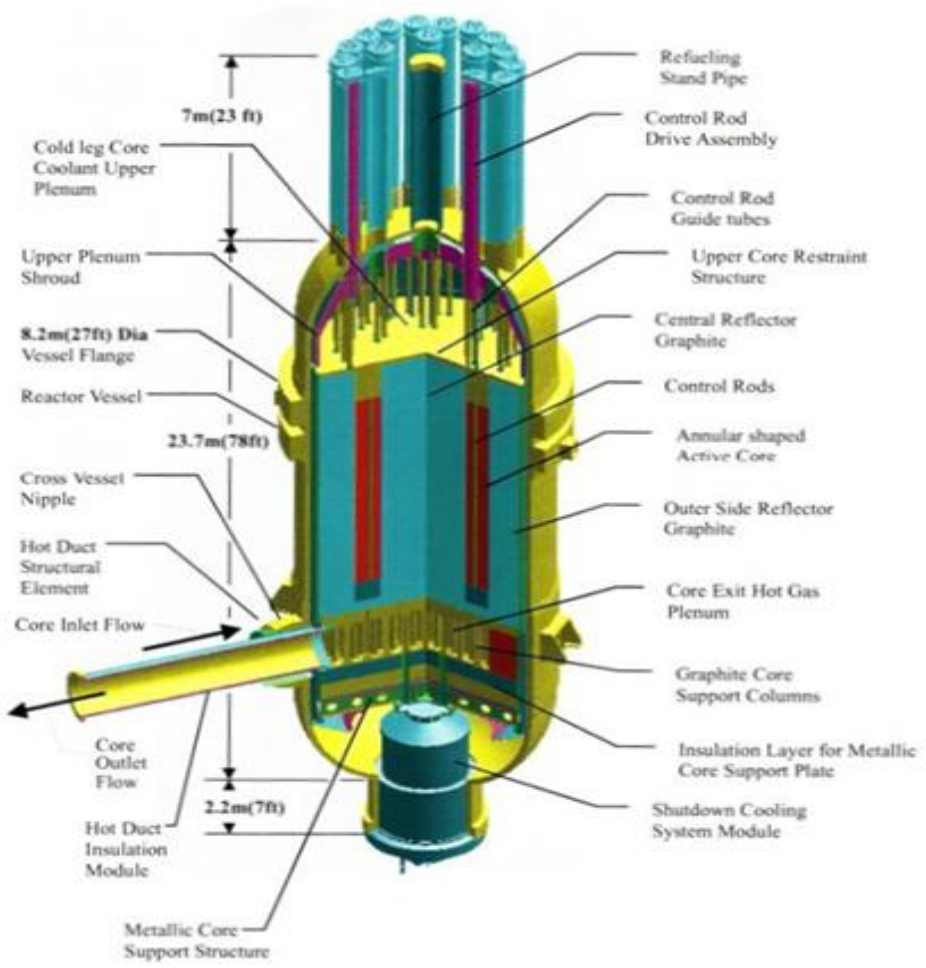

Figure 3-1: GT-MHR Diagram (2)

The lower part of the diagram shows the initial flow path of helium into the GT-MHR. Helium enters into the side of the reactor vessel's outer wall through the outer part of the coaxial duct in the bottom left of the figure, and then distributes radially around the core and into the upcomers. Once it travels through the upcomers it flows into the upper plenum and then down into the flow channels through the core and into the lower plenum. Once it enters the lower plenum it travels back out through the center of the annular duct. The reason that the flow is from the top of the reactor to the bottom is so that the cooler gas can keep the instrumentation and control rod drives from getting too

hot. The system pressure for normal operations is 6.375 MPa, with a core inlet temperature of 259 ºC with a core outlet temperature of 687 ºC.

3.1.2 MHTGR Geometric Characteristics (28)

The dimension of importance to this study, the distance between the top of the upper reflector and the center of the upper plenum shroud, which is referred to as the upper plenum height is 4.21 m. The upper plenum height is the maximum distance that the fluid entering the upper plenum from the core can travel before comes into contact with a direct obstruction

The center of the core is made up of the reflector, followed radially by a layer of mixed reserve shutdown control (RSC) elements and standard fuel elements, which is then followed by two layers of standard fuel elements. After the standard fuel elements are two layers of hexagon side reflectors, the first of which incorporates reactor control elements. After the hexagon side reflectors is the permanent side reflector, then the core wall.

With the exception of the flow channels around the fuel handling hole, which have a diameter of 12.7 mm (0.5 in), all of the coolant channels have a diameter of 15.875 mm (0.625 in). Within each fuel elements the fuel channels and coolant holes have a diameter of 18.795 mm (0.74 in). In the standard fuel element there are a total of 107 coolant channels per hexagon cell and in the RSC fuel element there are a total of 96 coolant channels per hexagon cell. With a total of 54 standard fuel elements and 12 RSC fuel elements, 6930 coolant channels resulting in a total flow area of 1.34 m^2. The upcomers are located between the inner and outer walls of the core.

3.2 High Temperature Test Facility

The OSU HTTF is a 2.2MWt integral scaled thermal hydraulic test facility, designed to be an electrically heated scaled model of the MHTGR. The scaling for this facility is ¼ axially and ¼ radially, which equates to 1/16 area scaling and 1/64 volumetric scaling. It will have a ceramic core with electric heater rods. The HTTF will operate at a reduced pressure compared to that for the MHTGR, 0.8 Mpa, which is approximately a 1/8 scale. It will operate at a temperature prototypical to that of the MHTGR. Additionally, the HTTF is designed to operate with helium or nitrogen depending on which matches the scaling parameters better for a particular test.

A computer rendered model of the HTTF can be seen in Figure 3-2.

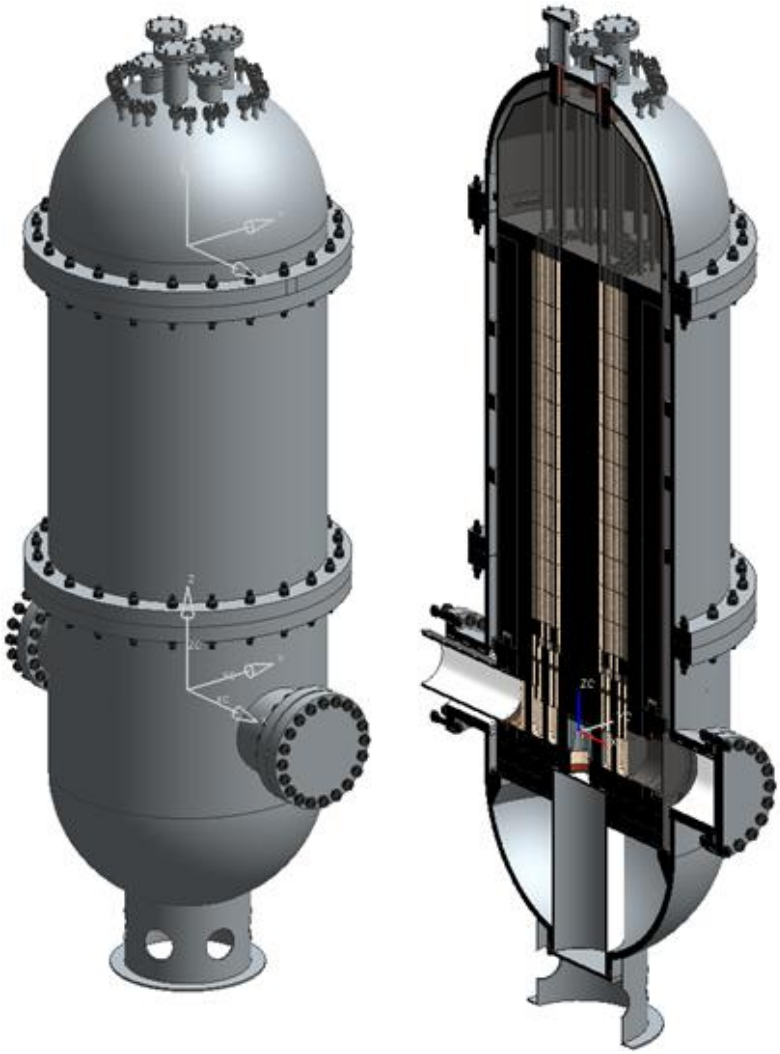

Figure 3-2: Oregon State University High Temperature Test Facility

The cutaway on the right shows the inlet-outlet crossover duct of the HTTF as well as the inside of the upper plenum and the flow channels that pass up through the core.

A top down view of the core can be seen in Figure 3-3.

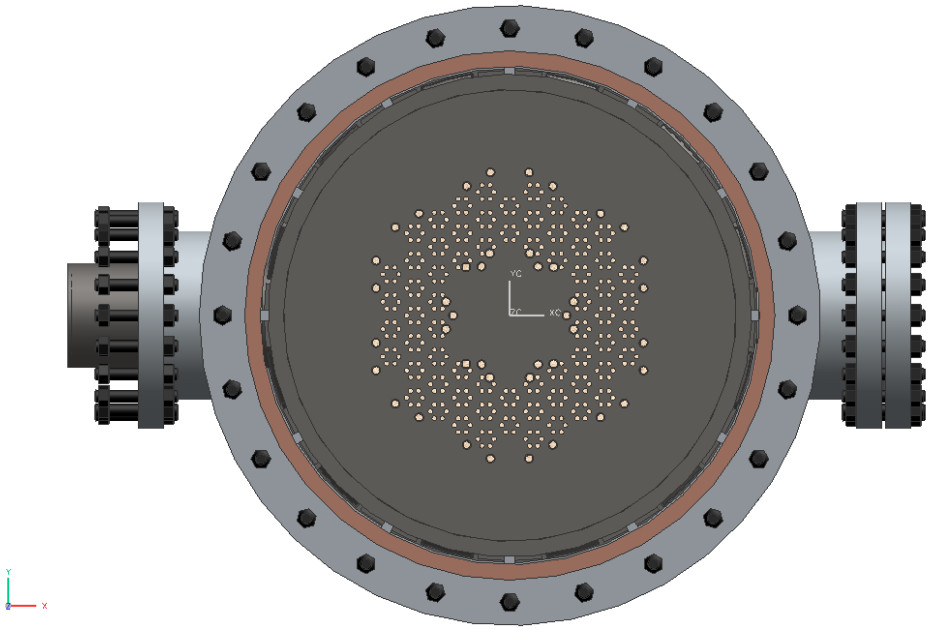

Figure 3-3: Top Down View of Core Flow Channels

The flow area for the HTTF is 1/16 of that of the MHTGR. This is achieved by maintaining the approximate flow channel size, but scaling down the number of flow channels so the layout is different than that of the MHTGR. In this top down view, the core flow channels can be seen in the center of the figure. With respect to the upper plenum, the end of these channels will act as the upper plenum inlets or outlets depending on the simulation. In order to scale the flow area of the HTTF, the flow channel diameter was maintained while the number of overall flow channels was reduced. This was done due to the difficulty of manufacturability of the smaller flow channels.

The flow pattern during normal operations of the HTTF is seen in Figure 3-4.

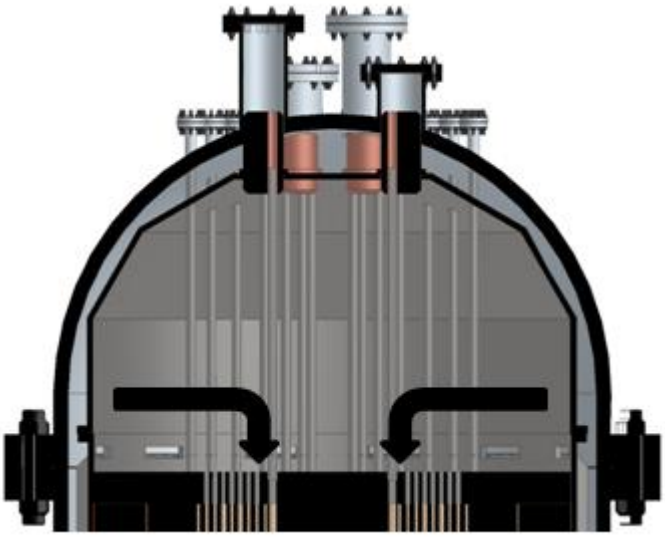

Figure 3-4: HTTF Normal Operations Flow Path

Like in the MHTGR, during normal operations, the coolant in the HTTF flows up through the upcomers in the wall of the reactor vessel into the upper plenum and down through the core.

3.3 Facility Summaries

The summary of the key properties for this study of the MHTGR and HTTF can be seen in Table 3-1.

Table 3-1: Facility Summaries

Property	MHTGR	HTTF
Coolant	Helium	Helium, Nitrogen
Operating Power (MWth)	350	2.2
Flow Area (m^2)	1.34	0.085
Upper Plenum Height (m)	4.21	1.05
Outlet Temperature (^oC)	687	687
Operating Pressure (MPa)	6.375	0.8

The operating power for the HTTF is its maximum operating power and will differ depending on the mode of operation.

4 Analytical Work

The following chapter details the analytical efforts to identify the necessary scaling parameters for this work. It also describes the derivations to determine the natural circulation velocities to be input into the scaling parameters. It then goes on to input the MHTGR and HTTF parameters to determine whether or not the facilities have any level of comparison from a scaling point of view.

4.1 Natural Circulation Velocity

The starting point for this analysis is the momentum equation in equation 1 written out in Cartesian coordinates,

$$\frac{\partial(\rho u_i)}{\partial t} + \frac{\partial \rho u_j u_i)}{\partial x_j} = (\Delta\rho)g + \mu \frac{\partial^2 u_i}{\partial x_j \partial x_j} \tag{1}$$

Each one of the terms in the equation is then normalized against the boundary of the inlet as seen in equations 2, 3, 4, 5, and 6,

$$\rho^+ = \frac{\rho}{\rho_{exit}} \tag{2}$$

$$\Delta\rho^+ = \frac{\Delta\rho}{\Delta\rho_{exit}} \tag{3}$$

$$u_i^+ = \frac{u_i}{U_{exit}} \tag{4}$$

$$t^+ = \frac{tU_{exit}}{L_{IP}} \tag{5}$$

$$x_i^+ = \frac{x_i}{d_{channel}} \tag{6}$$

where the + superscript notes the normalized ratio, U_{exit} is the velocity at the inlet of the upper plenum from the core, L_{IP} is the upper plenum length, and $d_{channel}$ is the flow channel diameter. Substituting these into equation 1 and multiplying out the terms attached to the time rate of change of momentum provides equation 7,

$$\frac{\partial(\rho^+ u_i^+)}{\partial t^+} + \frac{L_{IP}}{d_{channel}} \frac{\partial(\rho^+ u_j^+ u_i^+)}{\partial x_j^+} = \frac{\Delta\rho_{exit} g L_{IP}}{\rho_{exit} U_{exit}^2} (\Delta\rho)^+ + \left(\frac{\mu}{U_{exit}\rho_{exit} d_{channel}}\right)\left(\frac{L_{IP}}{d_{channel}}\right) \frac{\partial^2 u_i^+}{\partial x_j^+ \partial x_j^+} \quad (7)$$

Using the definitions of the densinometric Froude number and the Reynolds number shown in equations 8 and 9,

$$Fr = \left(\frac{U_{exit}^2 \rho_{exit}}{g L_{IP} \Delta\rho_{exit}}\right)^{\frac{1}{2}} \quad (8)$$

$$Re_d = \frac{\rho_{exit} U_{exit} d_{channel}}{\mu} \quad (9)$$

where the densinometric Froude number is defined as the ratio of the inertial to buoyant forces and the Reynolds number is the ratio of inertial to viscous forces, results a non-dimensionalized momentum equation seen in equation 10

$$,\frac{\partial(\rho^+ u_i^+)}{\partial t^+} + \frac{L_{IP}}{d_{channel}} \frac{\partial(\rho^+ u_j^+ u_i^+)}{\partial x_j^+} = \frac{1}{Fr^2} (\Delta\rho)^+ + \left(\frac{1}{Re_d}\right)\left(\frac{L_{IP}}{d_{channel}}\right) \frac{\partial^2 u_i^+}{\partial x_j^+ \partial x_j^+} \quad (10)$$

Depending on how the coordinates for this problem are evaluated, a length scaled Reynolds number could be used instead of the diametric Reynolds number. Looking at the diametric Reynolds number and the relationship between the upper plenum length and the channel diameter allows to analyze the effect of both characteristic lengths and the use of the length scaled Reynolds number is not needed. In this equation, the three key dimensionless numbers are the ratio of the inlet (upper) plenum length to flow channel diameter, $\frac{L_{IP}}{d_{channel}}$, the densinometric Froude number, Fr, and the length of the upper plenum divided by the diameter of the individual flow channels as well as the diametric Reynolds numbers, Re_d. Based on the way the equation is written, the Reynolds number and the ratio of inlet plenum length and flow channel diameter can be analyzed as a combined dimensionless number which will be identified in this work as a modified Reynolds number, $\frac{L_{IP}}{Re_d d_{channel}}$. In order to ideally scale the PCC phenomena between the two facilities, all three non-dimensional parameters would be matched between the two

facilities. The relationship between length and channel diameter is fixed between the systems at a one-to-four ratio, the diameter of the flow channels is roughly the same in both facilities, but the upper plenum of the MHTGR has a diameter that is four times larger.

The modified Reynolds number is shown, in equation 11,

$$Re_M = \frac{L_{IP}\mu}{\rho w_c d_{channel}^2} \tag{11}$$

The velocity in the Froude and Reynolds equations is the main variable parameter and is solved for in the following way, starting with the loop momentum balance equation shown in equation 12 below.

$$\Pi_{G,PCC}\frac{d\dot{m}_{loop}^{+}}{dt^{+}} = \Pi_{Ri,PCC}\left(\rho_{avg,c} - \rho_{avg,h}\right)^{+} - \Pi_{F,PCC}\frac{\left(\dot{m}_{loop}^{+}\right)^2}{\rho_{avg,loop}^{+}}\left\{\sum_{i=1}^{N}\left[\frac{1}{2}\left(\frac{fl}{d_h}+K\right)\left(\frac{a_{core}}{a_i}\right)^2\right]\right\}^{+} \tag{12}$$

In equation 4, $\Pi_{G,PCC}$ is the non-dimensional loop reference geometry number, $\frac{d\dot{m}_{loop}^{+}}{dt^{+}}$ is the change in flow rate through the loop, $\Pi_{Ri,PCC}$ is the Richardson number, $\rho_{avg,c}$ is the average density from the colder area and $\rho_{avg,h}$ is the average density in the hot area, $\Pi_{F,PCC}$ is the non-dimensional loop resistance number, $\dot{m}_{loop}^{+}$ is the mass flow rate, f is the frictional Darcy friction factor, l in the length of flow travel, d_h is the hydraulic diameter, K is the form loss, a_{core} is the overall core flow area and a_i is the area of the individual loop. This problem was evaluated at steady state, so the change in the flow rate goes to zero and the remaining all of the + terms go to unity leaving the three non-dimensional parameters. The loop reference geometry number goes away because there is only one loop for the system leaving the Richardson number and the non-dimensional loop resistance number equal to each other. They are shown in equations 13 and 14,

$$\Pi_{Ri,PCC} = \frac{g\left(\rho_{avg,c}-\rho_{avg,h}\right)L}{\rho_c w_c^2} \tag{13}$$

$$\Pi_{F,PCC} = \frac{\rho_{avg,c}}{\rho_{avg,loop}} \sum_{i=1}^{N} \left[\frac{1}{2} \left(\frac{fl}{d_h} + K \right) \left(\frac{a_{core}}{a_i} \right)^2 \right] \quad (14)$$

where $\rho_{avg,loop}$ is the loop average velocity. Continuing the derivation and replacing the change in density through the relationship of the thermal expansion coefficient, β, and then applying equation 15,

$$\dot{q} = \dot{m} C_p \Delta T \quad (15)$$

where $\dot{q}$ is the core thermal power, $\dot{m}$ is the core flow rate, C_p is the specific heat, and ΔT is the change in temperature across the core, and $\dot{m}$ isthe definition of mass flow rate shown in equation 16,

$$\dot{m} = \rho a_{core} w_c \quad (16)$$

where a_{core} is the area of the core. Putting all of this together, the natural circulation velocity is derived as shown in equation 17.

$$w_{avg,core} = \left(\frac{\beta_g g \dot{q} L}{\rho_{avg,core} a_{core} c_{p,avg} \Pi_F} \right)^{\frac{1}{3}} \quad (17)$$

Based upon information gained from previous studies (15) (16), and assuming that natural circulation has already begun resulting in a core temperature profile reversal, a lower core temperature of 300 K and an upper core temperature of 1000 K were utilized in this analysis. For the MHTGR, the power in this equation was set to 6% decay heat, which corresponds to 23MWth. An initial value of the velocity was used to calculate the friction factor. Once a velocity was calculated, the friction factor was recalculated and then the velocity again. This process was iterated upon until a velocity of 1.26 m/s was determined to be the natural circulation velocity. In the case of the HTTF, the velocity and power were calculated by determining the power and velocity ratio between the MHTGR and HTTF when temperature similarity is maintained. These ratios were determined using equations 15, 16 and 17. The simplified version of each of these equations can be seen in equations 18, 19 and 20,

$$(\dot{q})_R = \left(\dot{m}C_p\right)_R \tag{18}$$

$$(\dot{m})_R = (\rho a_{core} w_c)_R \tag{19}$$

$$\left(w_{avg,core}\right)_R = \left(\left(\frac{\dot{q}L}{\rho_{avg,core} a_{core} c_{p,avg}}\right)^{\frac{1}{3}}\right)_R \tag{20}$$

where the subscript R designates the non-dimensional relationship between the two facilities. In equation 18, the temperature change between the two facilities cancels out as temperature similarity is preserved. In equation 19, the parameters are different between each facility and nothing cancels out when setting up the non-dimensional ratio. In equation 20, the thermal expansion coefficient, and non-dimensional pressure loss are constant between the two facilities, which is the HTTF is designed to preserve. By then substituting equations 18 and 19 into equation 20, and cancelling out the specific heat, core area, and density, equation 21 is derived for the ratio of natural circulation velocity between the two facilities,

$$\left(w_{avg,core}\right)_R = \left(L_{IP}^{\frac{1}{2}}\right)_R \tag{21}$$

Inserting the ratio for natural circulation velocity between the two facilities back into equation 10 and along with equation 21 results in a non-dimensional ratio between the two facilities for power as seen in equation 22,

$$(\dot{q})_R = \left(\rho a L_{IP}^{\frac{1}{2}} C_p\right)_R \tag{22}$$

In the case of helium this would reduce further because temperature similarity would result in the specific heat for the two facilities being the same. From this analysis, the relative power and velocity for the HTTF when temperature similarity is maintained results in the velocities and powers for the two different gases in the HTTF as seen in Table 4-1.

Table 4-1: Power and Velocity for HTTF Under the PCC Event

Gas	Velocity (m/s)	Power (kW)
Helium	0.63	91
Nitrogen	0.63	149

Table 4-2: Reynolds, Froude and L/d for Natural Circulation Calculated Velocities

Facility	$\frac{L_{IP}}{d_{channel}Re_d}$	$\frac{1}{Fr^2}$	L/d
MHGTR	0.170	5.814	224
HTTF (Helium)	0.603	6.030	53
HTTF (Nitrogen)	0.777	5.926	53

For the Froude number calculation, an assumed 100 K temperature change between the core and the upper plenum was defined based on information from previous studies (15). Just looking at the disparity in the numbers, it's clear that the Reynolds and Froude numbers do not match. The distortion can be calculated using equation 23.

$$Distortion = \left|\frac{\Pi_{MHTGR}-\Pi_{HTTF}}{\Pi_{MHTGR}}\right| \times 100 \quad (23)$$

where Π_{MHTGR} is any non-dimensional number calculated for the MHTGR and Π_{HTTF} is the same non-dimensional number that has been calculated for the HTTF.

The distortions calculated for these two cases can be seen below in Table 4-3.

Table 4-3: Natural Circulation Distortion

Gas	$\frac{L_{IP}}{d_{channel}Re_d}$	$\frac{1}{Fr^2}$	L/d
Helium	253	3.72	76.3
Nitrogen	354	1.93	76.3

4.2 Forced Circulation Velocity

As mentioned in section 4.1 it is possible to run the blowers of the HTTF to result in forced circulation of the Helium. The downside to this is that the effect of the blowers

will leave all of the HTTF channels in upward circulation, which would allow only for the analysis of the inlet/outlet duct crossover break scenario. To determine the velocity required for forced circulation, the modified Reynolds number for the HTTF was set equal to the MHTGR and the velocity required to match the two non-dimensional numbers was calculated by solving for the velocity on the HTTF side. Because the Froude number matches with the natural circulation velocity, this analysis was only performed for the modified Reynolds number. The results of these two cases can be seen below in Table 4-4.

Table 4-4: Forced Convection Distortion

Gas	Velocity (m/s)	$\frac{L_{IP}}{d_{channel}Re_d}$	$\frac{1}{Fr^2}$	$\frac{L_{IP}}{d_{channel}Re_d}$ distortion	$\frac{1}{Fr^2}$ distortion
Helium	2.24	0.170	0.037313	0	15400

As can be seen, when the modified Reynolds number is matched a large distortion occurs in the Froude number term, as it did in the Reynolds term when the Froude number term was well matched.

4.3 Summary

This section was responsible for determining the operating velocities for the PCC event for the MHTGR as well as the PCC event under natural circulation and forced convection with both helium and nitrogen.

A summary of these velocities can be seen below in Table 4-5.

Table 4-5: Velocities for Natural Circulation and Convection during PCC Event

Facility	Gas	Mode of Flow	Velocity (m/s)
MHTGR	Helium	Natural Circulation	1.26
HTTF	Nitrogen	Natural Circulation	0.63
HTTF	Helium	Natural Circulation	0.63
HTTF	Helium	Forced Convection	2.24

These velocities set up the inlet conditions for the next step in this analyses, computation fluid dynamics modeling (CFD) of the problem using Star-CCM+.

5 Star-CCM+ Computational Fluid Dynamics Modeling

This section details the models developed for use in Star-CCM+ to analyze the PCC fluid flow phenomena in the upper plenum of both the HTTF and the MHTGR. These models have been designed to visually assess the fluid behavior during the PCC event in the upper plenum as well as examine the effects of the reduced scale on the fluid behavior.

5.1 Continuity and Momentum Equations

Star-CCM+ operates by using the three continuity equations: mass, momentum and energy. Star-CCM+ evaluates them through finite volume discretization. All three are solved simultaneously by implementing the coupled flow and coupled energy models. The coupled flow then gives the choice of integration and discretization methods, for which implicit and second order upwind were chosen. The 2^{nd} order upwind method was used due to the numerical diffusion that would be introduced by the use of a 1^{st} order method. The implicit method was chosen because it provides a wider stability margin; however, this does require more system storage than the explicit scheme. In order for these models to be solved, a series of other models are used to describe the physics that affect the three equations and must be implemented in Star-CCM+ which include a gas model, gravity and three dimensional models. All models were determined to be in laminar flow and thus laminar flow models were used.

5.2 Geometric Models

The geometry used for the MHTGR can be seen in Figure 5-1.

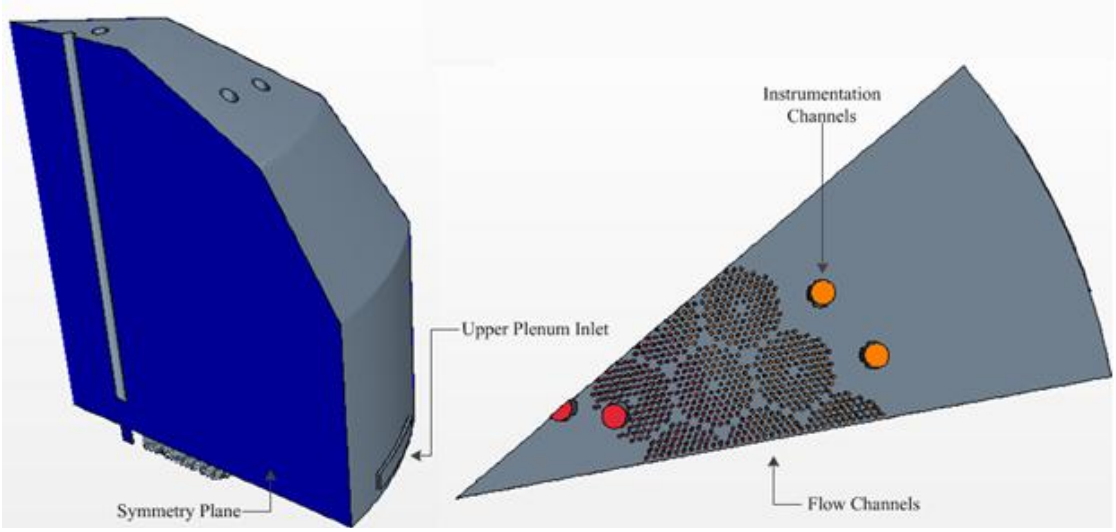

Figure 5-1: Star-CCM+ MHTGR Geometry

The left part of the figure shows the overall view of the MHTGR's upper plenum. At the back on the left can be seen the normal operations inlet to the upper plenum from the upcomers. The right part shows a bottom up view of the upper plenum. A $1/12^{th}$ slice was used for this model due to computational constraints. This $1/12^{th}$ slice was able to be utilized through the symmetry plane that is seen the figure. The symmetry plane also exists on the other side of the slice. Each one of the flow channels, as well as the instrumentation channel picture can be operated in up or down flow. For the purposes of modeling, they are lumped into radial categories, where the first 25% of the channels are the first region, the second 25% of the channels are the second region and the last 50% of the channels one region.

The Star-CCM+ models for the HTTF can be seen in Figure 5-2.

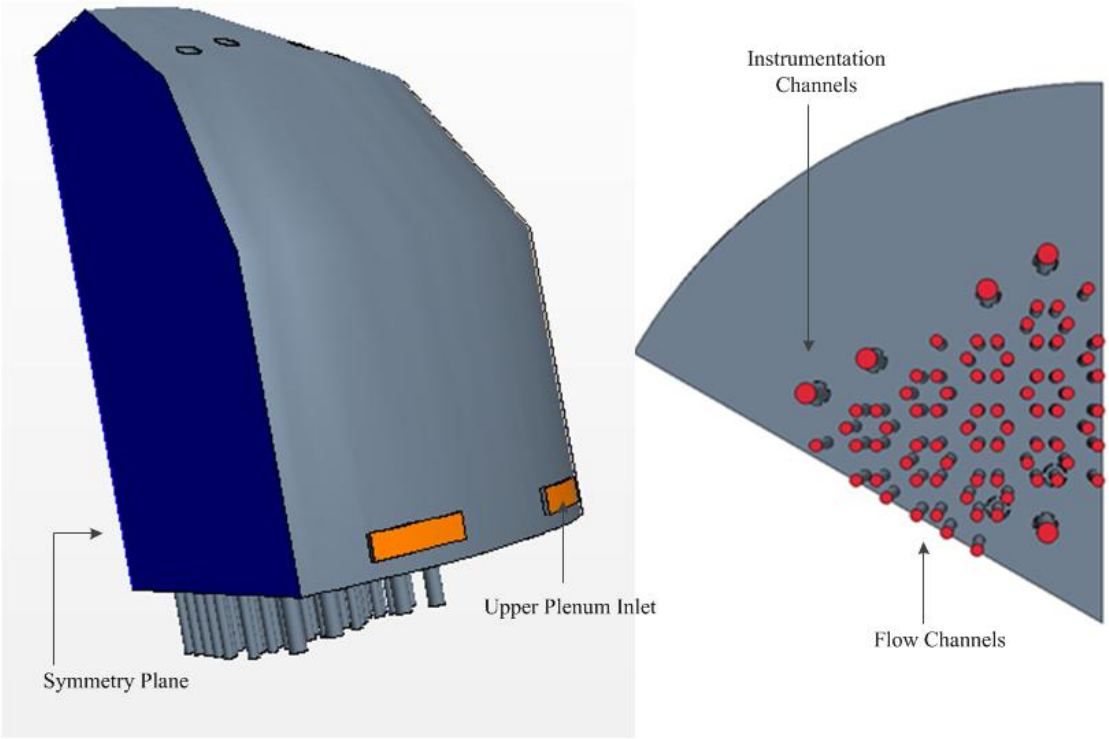

Figure 5-2: HTTF Star-CCM+ Models

The view on the left shows a translucent view of the upper plenum for the HTTF. The bottom two openings on the back are the upper plenum connection to the upcomers. The five channels that travel through the upper plenum are instrumentation channels and extend into the core as flow channels and bypass channels. On the right is shown a bottom up view from the core of the flow channels into the HTTF. The radial rings of the HTTF are designated in the same way as in the MHTGR model.

5.3 Initial and Boundary Conditions

During the complete loss of flow scenario, it is expected that the hotter inner regions of the core will operate in upflow and the cooler outer regions will operate in down flow. A sensitivity study was run for three different types of upflow to look at various possibilities for what might affect the flow patterns in the upper plenum depending on how many of the flow channels are in upflow and how many are in downflow. These

cases are with the first 25%of the channels radially in upflow with the rest of the channels in downflow and the outlet closed, the first 50% of the channels in upflow with the rest of the channels in downflow, and all of the channels in upflow with the outlet open. Due to the location of the sink with respect to the heat source, it is not postulated that all of the flow channels will operate in upflow with downflow down the upcomer, but using this model with the capabilities of the HTTF to run the blower in reverse allows for evaluating the effects of matching the modified Reynolds number.

A sum of all of the test cases can be seen in Table 5-1.

Table 5-1: MHTGR and HTTF Testing Matrix

Trial Number	Facility	Gas	Entrance Velocity (m/s)	Percent Channels Upflow
1	MHTGR	Helium	1.26	25
2	MHTGR	Helium	1.26	50
3	MHTGR	Helium	1.26	100
4	HTTF	Helium	0.63	25
5	HTTF	Helium	0.63	50
6	HTTF	Helium	0.63	100
7	HTTF	Nitrogen	0.63	25
8	HTTF	Nitrogen	0.63	50
9	HTTF	Helium	2.24	100

The pressure in the system is initially set to operating pressure of each facility, 6.375 MPa for MHTGR and 0.8 MPa for the HTTF. The outlets are set to what Star-CCM+ calls pressure outlets, which prevent flow below the pressure outlet setting from crossing the boundary. The value for the pressure outlets is the same as that of the system pressure to prevent the flow from building up inside the vessel and to prevent the vessel from becoming a vacuum. The temperature for the inlets is set to that as defined in the previous chapter with the 100 degree lower temperature being set for the top of the upper plenum head to a constant value to a constant value to allow for the natural circulation flow. The sides of the slices of both models operate as symmetry planes, which mean that the problem acts as a mirror image of itself over these planes which allows the use of slices of the domain to minimize computer requirements. They do not act as physical

boundaries that confine the fluid itself, that is to say that they do not act as walls to keep the fluid in but they do not add any frictional resistance to the flow. The remaining walls are treated as isothermal so that no heat transfer occurs across them.

5.4 Mesh Conditions

The MHTGR and HTTF were meshed differently because of their size; however, the same models were used. The first model is a polyhedral mesh model which is designed to be easy and efficient and contain five times less cells than a tetrahedral mesh with the same surface size. The polyhedral mesh model is used in the creation of the volume mesh. The second model used, the surface remesher is used to re-triangulate surfaces to improve overall efficiency for volume meshing. The final mesh model used is the prism layer mesh. It adds orthogonal prismatic cell along wall boundaries which allow for better simulation along those boundaries.

For the MHTGR model, a base size of 0.035 m was used. This resulted in 1022798 cells. A picture of the MHTGR mesh can be seen in Figure 5-3.

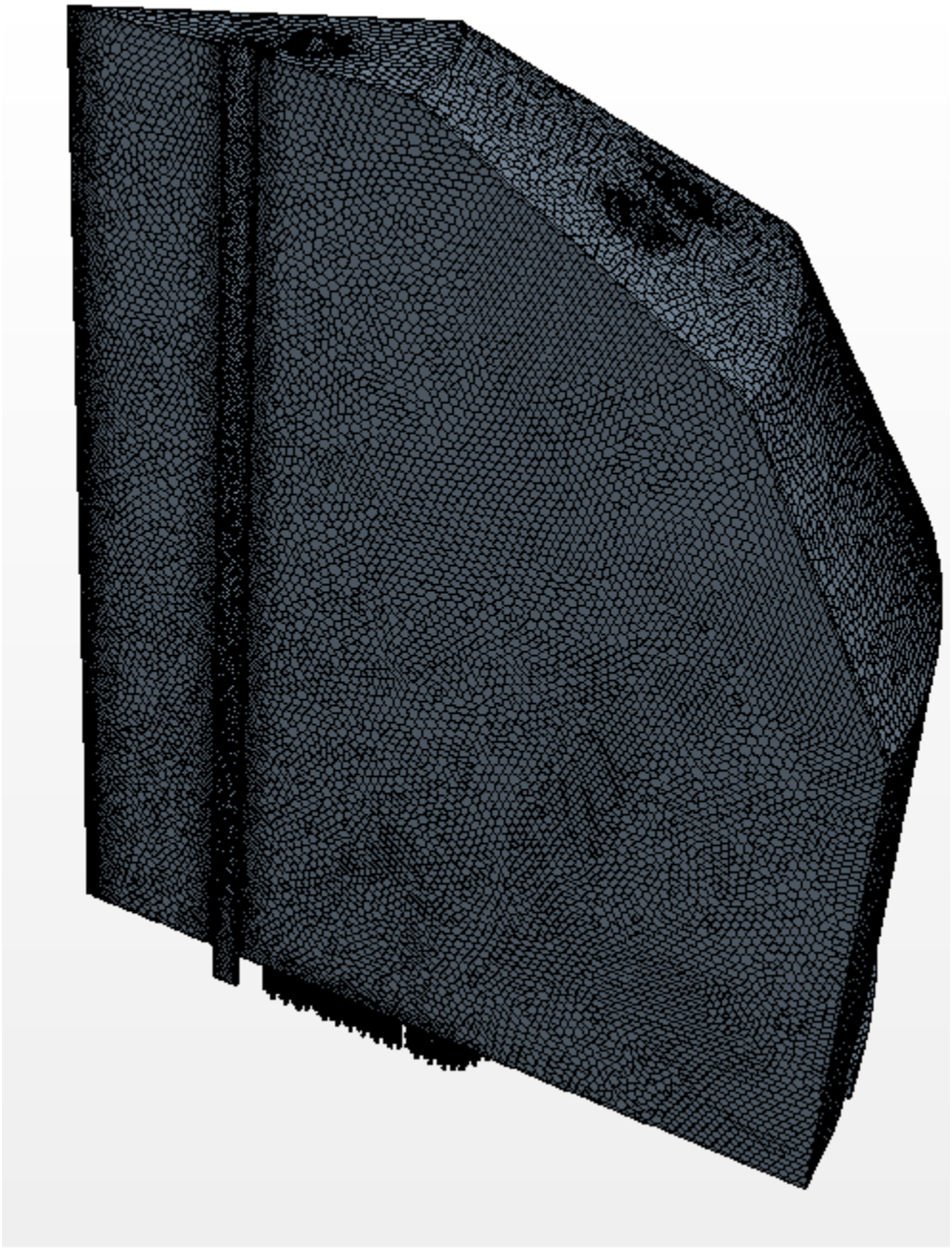

Figure 5-3: MHTGR Mesh

The HTTF model was built with a base size of 0.0225m, which resulted in 297290 mesh volumes. It can be seen in Figure 5-4.

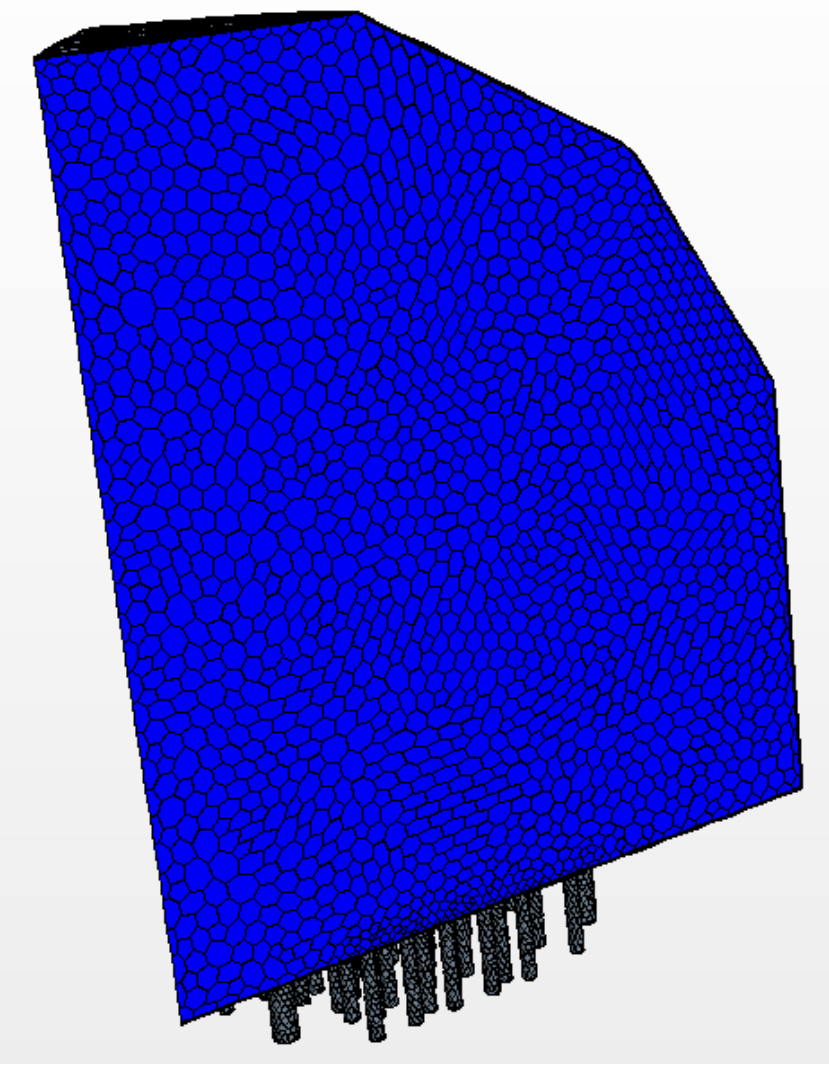

Figure 5-4: HTTF Mesh

5.5 Physics Models

A series of physics models were used. First, the three dimensional physics model was enabled. Since the body was modeled as a fluid model with helium or nitrogen depending on the test, the gas model was chosen under the material option. The gravity

model was implemented as this is a natural circulation model and the effects of gravitation acceleration are needed to accurately model the forces present in natural circulation flow. Because the intention is to model this as a steady state problem the steady model was chosen under the time options. The coupled flow model was chosen which solves the conservation of mass and momentum equations simultaneously with a 2^{nd}-order implicit scheme. The coupled energy model was added to this so that the conservation of energy will be solved with the other two continuity equations.

6 Star-CCM+ Results and Analysis

This chapter will present the results of the Star-CCM+ models developed in chapter 5 as well as the analysis of these models. Each section will detail the four results that stem from the same inlet conditions with the three upflow to downflow ratios. The first thing in each section that will be presented is the MHTGR simulations. Following that the results from the various HTTF simulations will be presented as well as their individual comparisons to the MHTGR simulations. Two metrics have been identified to determine the scaling comparison between the MHTGR and HTTF simulations: 1) distance into upper plenum gas jets travel before diffusion and 2) comparison of temperature profile. In order to compare the temperature profile, various properties were analyzed. First, a visual inspection of the temperature profile was performed. Second, measurements were taken of the average temperatures on three horizontal slices in the upper plenum at distances 30%, 45% and 72% of the distance into the upper plenum, as well as the maximum temperature on these planes as well as the minimum temperature. The average temperature plane temperatures give an idea of how much energy is transferred from the core to the upper plenum, the higher the temperature, the more heat is being transferred into the upper plenum. The maximum and minimum temperature allow for an idea of how well mixed the upper plenum is, the closer these two temperature are, the more mixing has occurred. These two temperatures were found by placing a line probe in the upper plenum on the three temperature planes.

6.1 Grid Refinement

In order to determine if grid independence was achieved the first MHTGR and first HTTF cases were evaluated. In order to determine grid independence, a superfine grid size was compared to the grid size that was initially evaluated. In order to evaluate this difference equation 24 was used,

$$\%\ difference = \frac{|p_1 - p_2|}{p_1} x100 \quad (24)$$

where p_1 is the value of any property measured a given point in the mesh volume of the coarser mesh and p_2 is any the same property measured at the same point in the finer mesh volume.

In the case of the HTTF, trial 5 was evaluated, with a course mesh of 297,290 nodes and a fine mesh of 422,152 nodes. Comparisons were made with the average temperature on temperature planes and a maximum percent difference of 0.000697% was seen. From this, it was determined that the HTTF solutions were grid independent.

Due to computational constraints a finer mesh was not evaluated in the same way for the MHTGR.

6.2 25% Upflow Simulations

This section deals with the 25% upflow simulations for the MHTGR and HTTF which consists of runs 1, 4 and 7. Two figures will be presented for each simulation run: temperature profile and velocity vector. First the MHTGR simulation results will be presented and then analyzed, followed by the HTTF and then the comparisons between them.

The first simulation presented is for Trail 1, the 25% upflow case for the MHTGR, with the temperature profile presented in Figure 6-1.

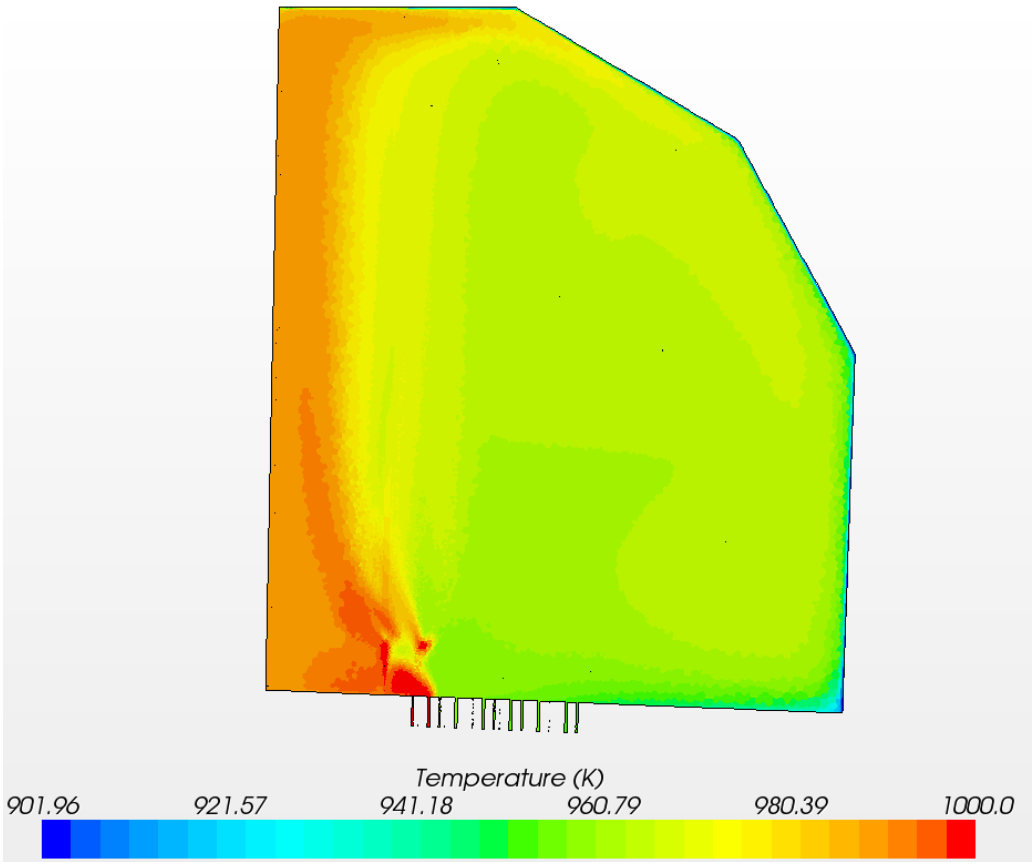

Figure 6-1: Trial 1 Temperature Profile

The gas jets enter into the upper plenum through the channel closest to the center of the upper plenum at 1000 K. They lose heat as they diffuse and travel towards the center of the upper plenum and begin to mix with the overall upper plenum, finally reaching the upper plenum wall at around 990 K. When they enter the upper plenum, the gas jets preferentially travel towards the inner most part of the upper plenum. The temperature in gas jets decreases the further they are away from the center of the upper plenum until they reach the bulk region.

The maximum temperature on the three temperature planes ranges from 990.56 K at the highest temperature plane to 991.53 K on the lowest temperature plane. The lowest

temperature on those planes ranges from 962.42 K on the lowest plane to 965.72 K on the highest plane.

The average temperature on the three temperature planes from bottom to top are 964.40, 965.70 and 967.28 K.

The next figure presented, Figure 6-2 shows the velocity vectors for Trial 1.

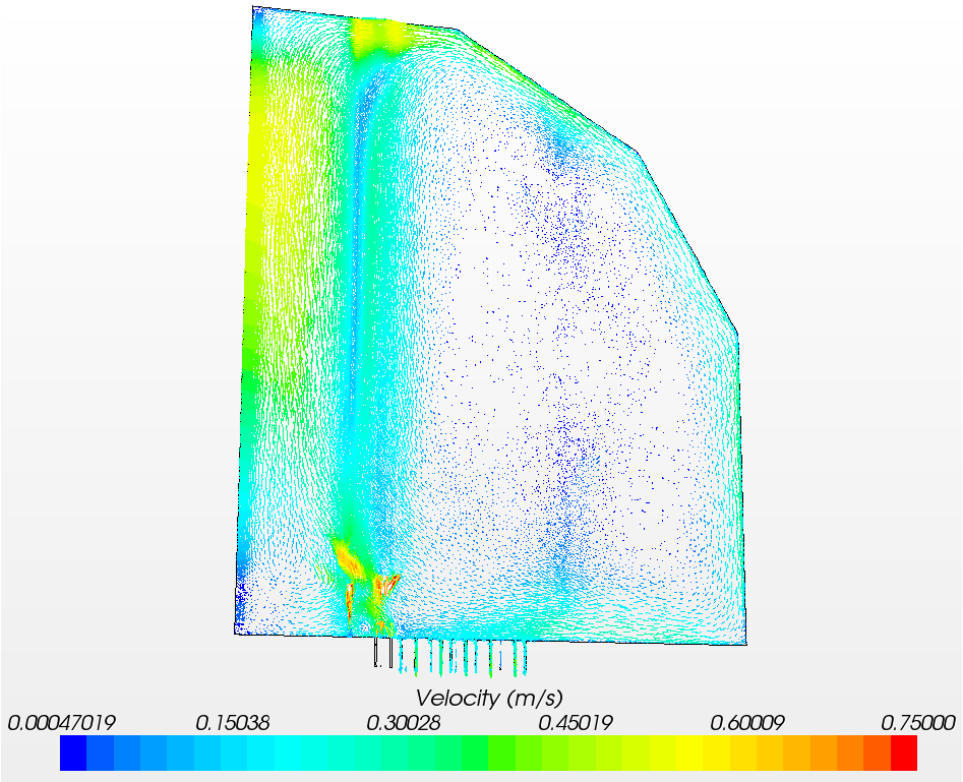

Figure 6-2: Trial 1 Velocity Vector

Upon entering the upper plenum, the gas drops to below its initial velocity as it diffuses into the upper plenum and the gas jets initially concentrate and the gas jets closest to the center accelerate as they move towards the center of the upper plenum until the come into contact with the top of the upper plenum and redirect along the outer wall until they leave the upper plenum through the outlet channels. As the gas travel around the upper plenum head some of them leave the upper plenum through the outlet channels, while others

come into contact with the incoming jets and recirculate in the upper plenum. This recirculation results in the incoming gas jets being pushed towards the center of the upper plenum. This pushes the gas jets in between the center of the upper plenum and the center instrumentation channel. This creates an effective flow channel at the center of the upper plenum where the gas jets accelerate as if they were traveling through a pipe, where the instrumentation channel acts as a wall. Those jets closets to the instrumentation channels are at the lowest velocity with the jets furthest away at the center of the upper plenum at the higher velocity. Additionally, the gas jets on the outer part of the instrumentation channel away from the center also see this effect except to a smaller degree as they are open to a larger bulk region. The gas jets continue to form this channel like flow until they reach the upper plenum where after coming into contact with the upper plenum are redirected along the upper plenum head. As they travel along the upper plenum head they then travel between the instrumentation channels resulting in them accelerating again as they have to converge to travel through them resulting in their acceleration. This is seen again further down the upper plenum but at a slower rate because the space between the instrumentation channels in the outer part of the upper plenum is larger. The gas then travels to the lower part of the upper plenum where some of it leaves through the outlet channels while the rest either diffuses into the non-flowing bulk of the upper plenum or comes into contact with the incoming gas jets and recirculates into the upper plenum.

The next figure, Figure 6-3, is the temperature profile for the first 25% upflow HTTF case, trial 4.

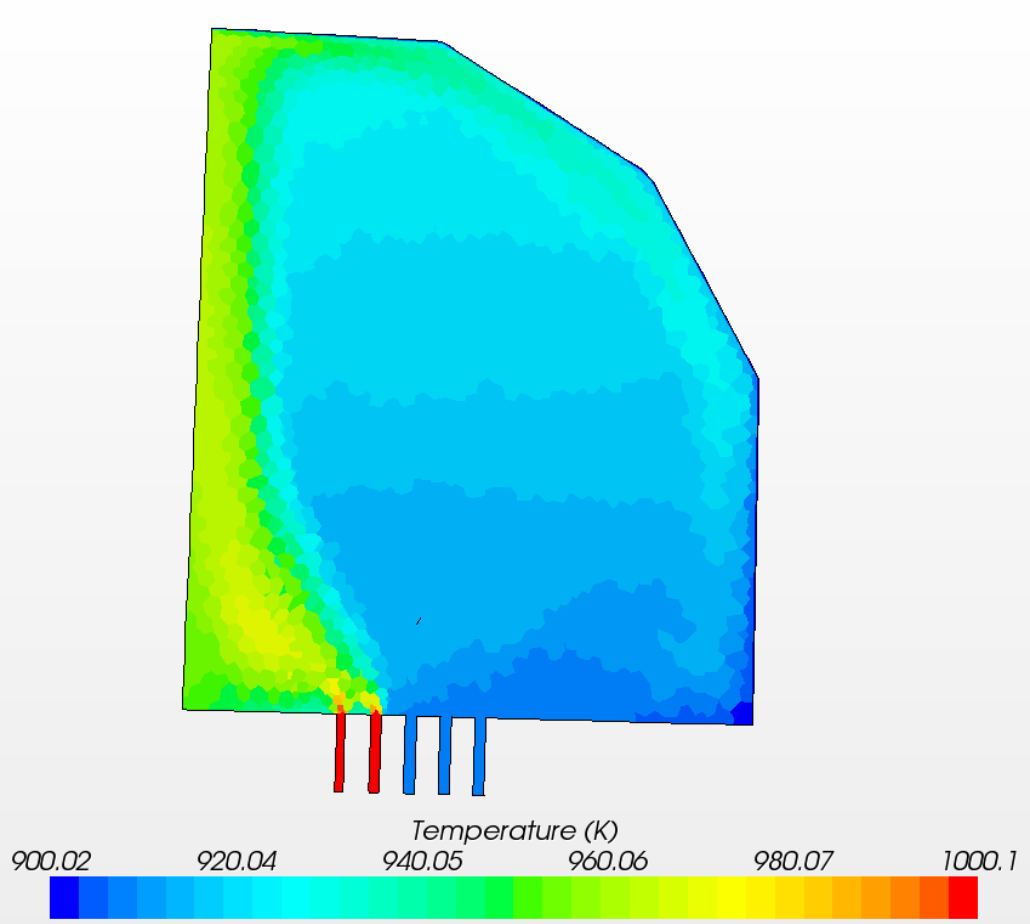

Figure 6-3: Trial 4 Temperature Profile

The gas jets enter through the upper plenum through the channel closest to the center of the upper plenum at 1000 K. They lose heat as they diffuse and travel towards the center of the upper plenum and begin to mix with the overall upper plenum, finally reaching the upper plenum below 960 K.

The maximum temperature on the three temperature planes ranges from 962.00 K at the highest temperature plane to 964.23 K on the lowest temperature plane. The lowest temperature on those planes ranges from 915.19 on the lowest plane to 918.44 K on the highest plane.

The average temperature on the three temperature planes from bottom to top are 916.72 K, 919. 65 K, and 925.87 K.

The next figure presented, Figure 6-4, is the velocity vector for the trial 4 case.

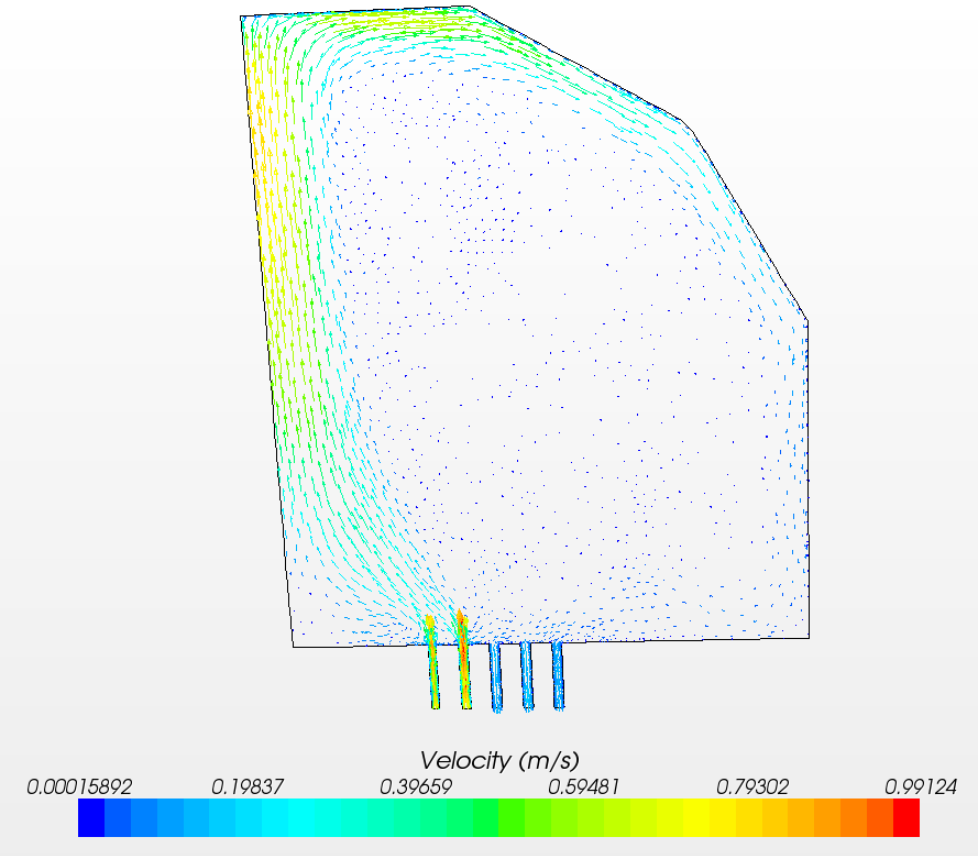

Figure 6-4: Trial 4 Velocity Vector

A very similar overall flow is seen in both trial 1 and in trial 4. As the gas jets enter the upper plenum in trial 4 they direct towards the very center of the upper plenum and exhibit the same overall characteristics as seen in trial 1. As they travel up the center region of the upper plenum, the geometry is the same resulting in the same acceleration of the flow due to the channeling in the same three areas. In both the trial 1 and trial 4

cases, the gas jets reach the upper plenum at the highest point in the center of the upper plenum before redirecting along the upper plenum wall and out of the upper plenum. There is not nearly as much recirculation in the case of trial 4 and the overall velocities in those channels are higher than in trial 1. The main reason for the higher velocities is that there is less mixing in trial 4 than in trial 1, which results in the lateral forces of the fluid imparting less force on the fluid than in the trial 1 case.

They have significantly different temperature profiles. The trial 1 average temperatures are as much as 47 K higher than in trial 4, while the range of temperatures for trial 1is between 24.84 and 29.11 K as compared to trial 4 which is between 39.00 K and 49.07 K. From these range of temperatures in the two cases it can be seen that although the gas jets reach the same point in the upper plenum in both cases, there is more mixing in the trial 1 case. It should be noted that while there is more mixing in trial 1, the overall temperatures in the HTTF are lower. Because both the axial and radial dimensions are scaled ¼, it results in the HTTF having a four times larger surface area to volume ratio which allows better heat transfer between the upper plenum head and the gas in the upper plenum. It should be noted, that although the flow path remain the same, the velocities seen in the HTTF case are faster than those in the MHTGR which does not stay consistent with the velocity scaling.

The next figure presented, Figure 6-5, is the temperature profile for the trial 7 case.

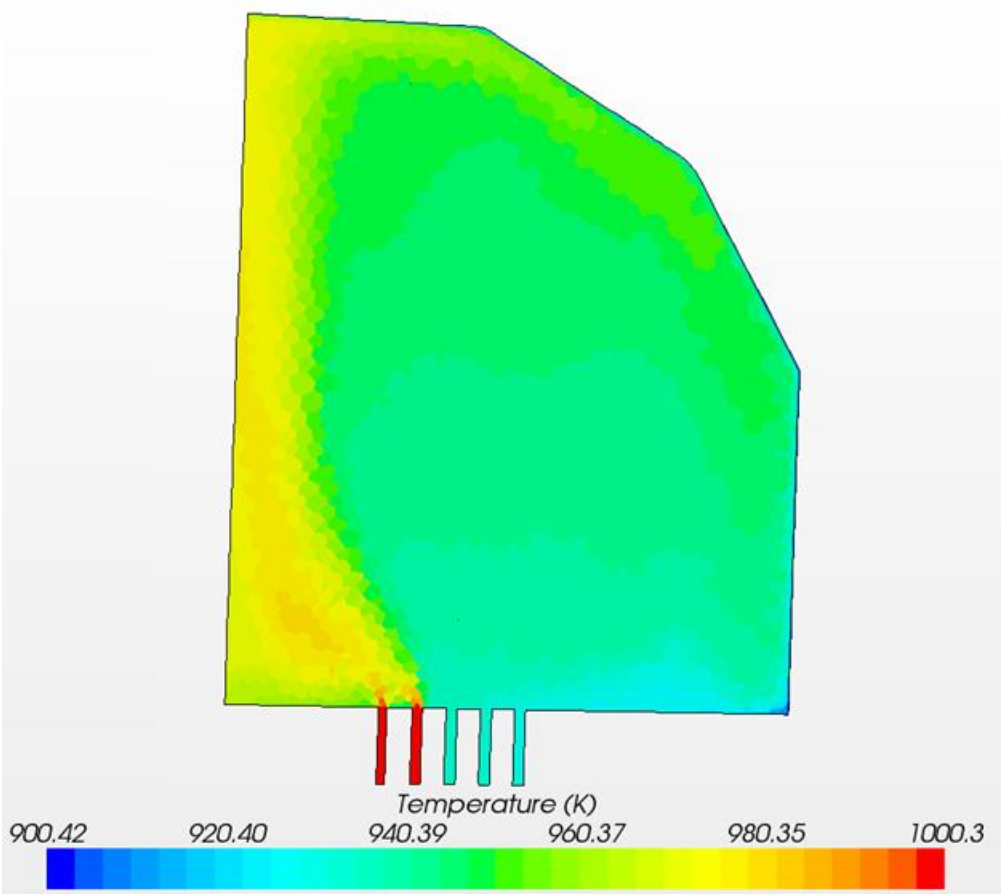

Figure 6-5: Trial 7 Temperature Profile

Similar behavior is seen in the trial 7 as in the trial 4, except with higher temperatures. In trial 7 the gas jets come into contact with the upper plenum at around 970 K.

The maximum temperature on the three temperature planes ranges from 974.83 K at the highest temperature plane to 964.23 K on the lowest temperature plane. The lowest temperature on those planes ranges from 942.08 K on the lowest plane to 943.76 K on the highest plane.

The average temperature on the three temperature planes from bottom to top are 942.97 K, 944.94 K and 949.54 K.

The next figure presented, Figure 6-6, is the velocity vector for trial 7.

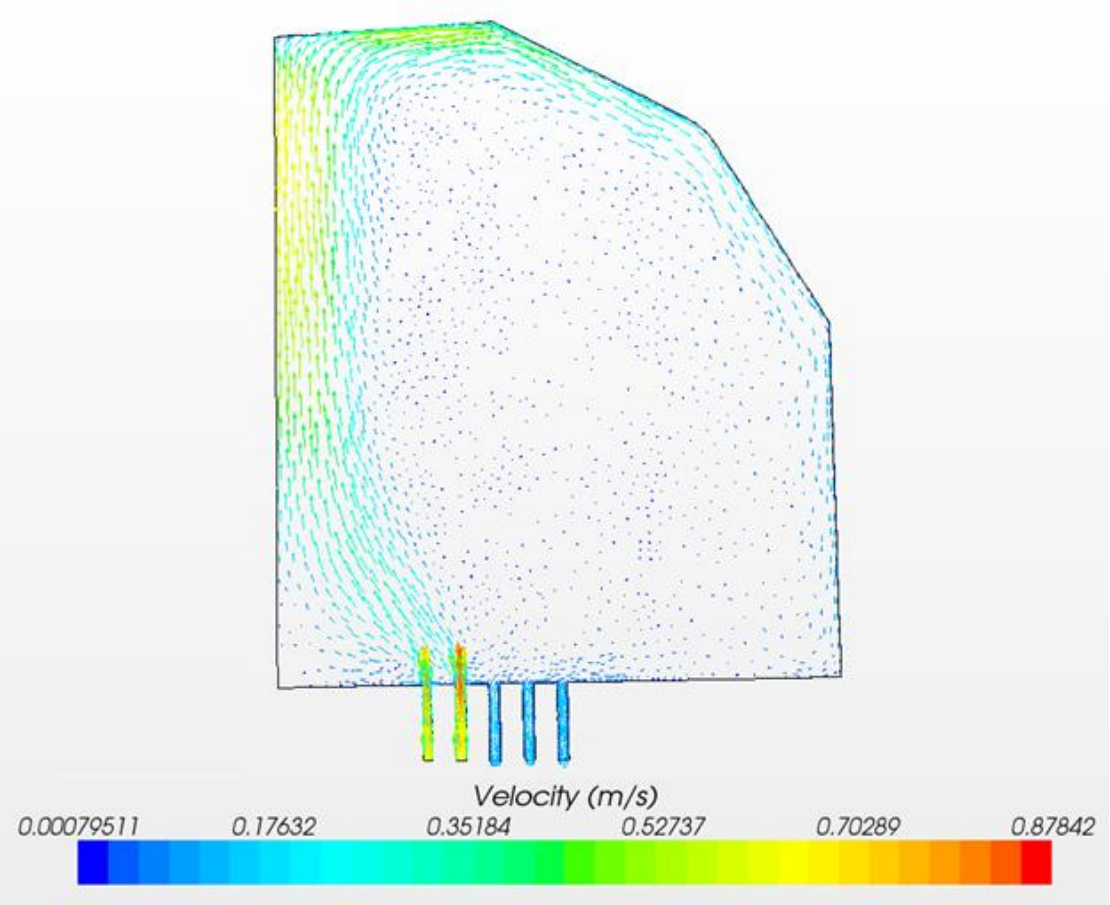

Figure 6-6: Trial 7 Velocity Vector

The same general behavior is seen in the trial 7 velocity vectors as in the trial 4. Again, the gas jets redirect towards the center region of the upper plenum and acceleration of the flow is seen in the same locations.

The same comparisons can be drawn from the trial 4 case to the trial 1 case as can be from the trial 7 case to the trial 1 case, except that in the trial 7 case the temperatures are higher and the velocities lower than in trial 4. There is more mixing in trial 7 in trial 4 which results in the lower velocity. The trial 1 average temperatures are as much as

21.43 K higher than in trial 7, while the range of temperatures for trial 1 is between 24.84

55and 29.11 K as compared to trial 7 which is between 27.94 K and 34.26 K. As in trial 4, the overall temperatures in the upper plenum are lower in trial 7 than trial 1 from the increased heat transfer rate.

As compared to trial 1, the mixing in trial 7 is closer to what is seen in trial 1 than was seen in trial 4; however, the overall temperatures are still much lower than those of trial 1.

6.3 50% Upflow Simulations

This section details the results for the 50% upflow cases.

The first figure in this section is Figure 6-7, which is the temperature profile for trial 2.

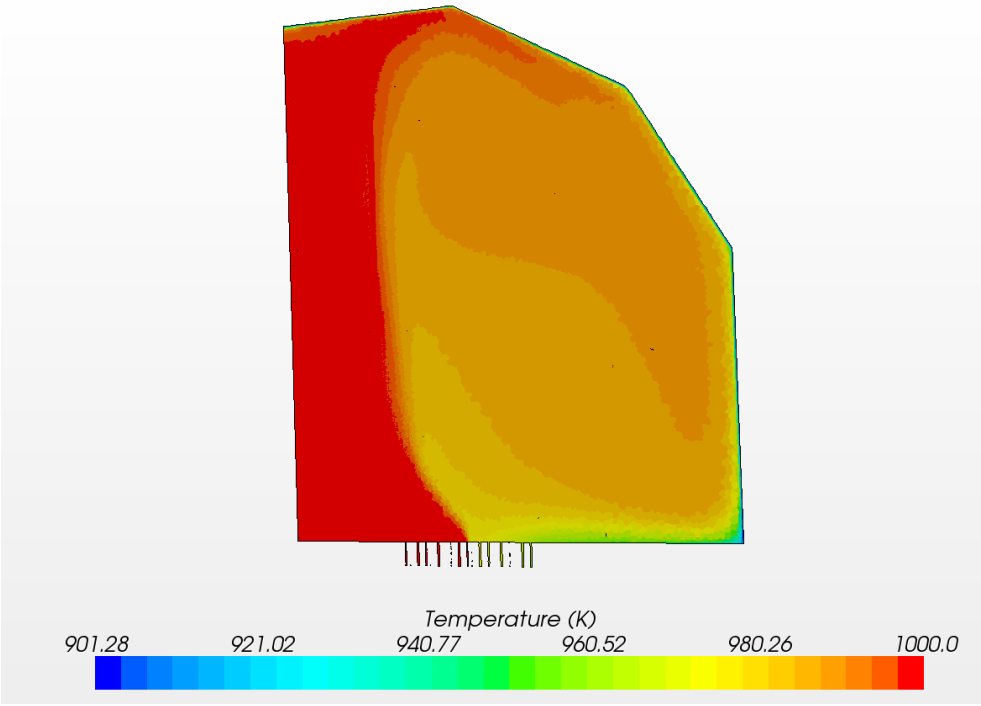

Figure 6-7: Trial 2 Temperature Profile

The gas jets enter through the upper plenum through the channel closest to the center of the upper plenum at 1000 K. They lose heat as they diffuse and travel towards the center of the upper plenum and begin to mix with the overall upper plenum, finally reaching the upper plenum at around 1000 K.

The maximum temperature on the three temperature planes ranges are all 1000 K on the lowest temperature plane. The lowest temperature on those planes ranges from 983.76 K on the lowest plane to 988.90 K on the highest plane.

The average temperature on the three temperature planes from bottom to top are 986.26 K, 986.80 K, and 988.61 K.

The next figure, Figure 6-8, is the velocity vector for trial 2.

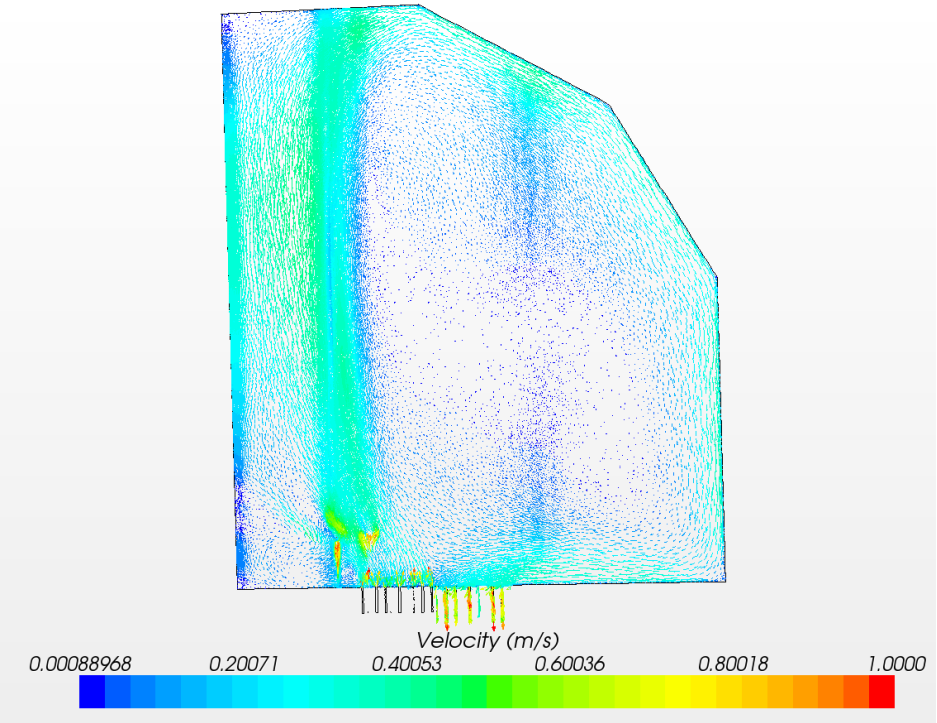

Figure 6-8: Trial 2 Velocity Vector

Upon entering the upper plenum, the gas drops to below its initial velocity as it diffuses into the upper plenum and the gas jets initially concentrate as they move towards the center of the upper plenum until the come into contact with the top of the upper plenum and redirect along the outer wall until they leave the upper plenum through the outlet channels. The same overall behavior is seen in in trial 2 as was seen in trial 1, with the main difference coming from the larger amount of gas flowing into the upper plenum. With 50% more gas jets flowing into the upper plenum, the overall temperature is higher and the amount of recirculation is higher.

The next figure presented, Figure 6-9, is the temperature profile for trial 5.

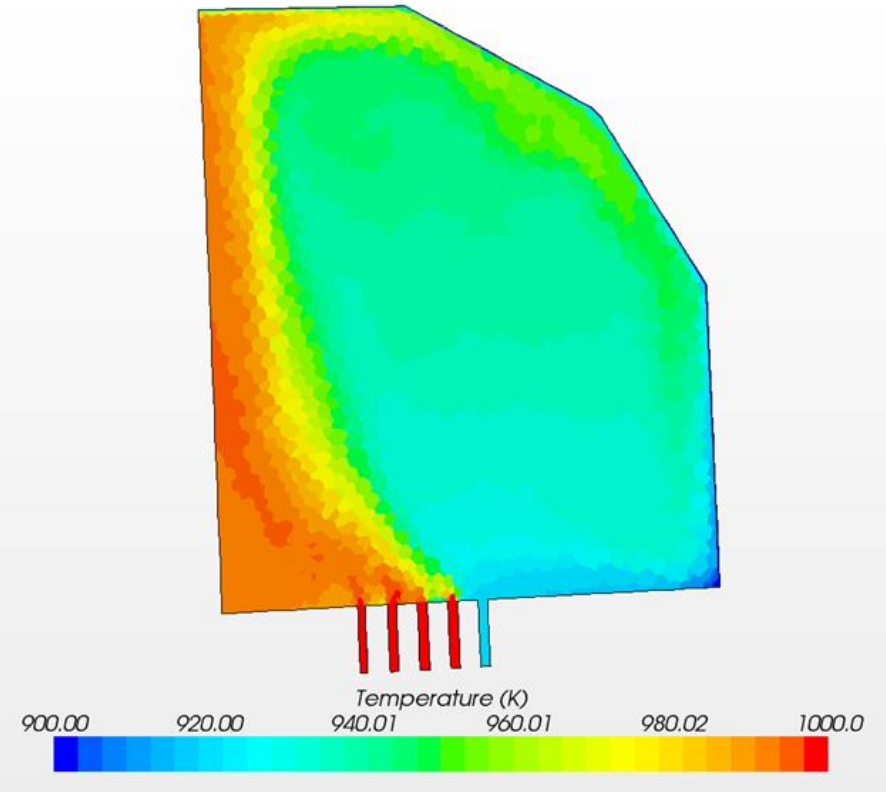

Figure 6-9: Trial 5 Temperature Profile

The same behavior is seen in the trial 5 temperature profile as was seen in the trial 4 temperature profile, except that due to the extra upflow channels in trial 5, the temperatures in the upper plenum are higher. The gas jets reach the upper plenum at a temperature just above 980 K.

The maximum temperature on the three temperature planes ranges from 991.90 K at the highest temperature plane to 994.08 on the lowest temperature plane. The lowest temperature on those planes ranges from 933.86 on the lowest plane to 942.81 K on the highest plane. The average temperature on the three temperature planes from bottom to top are 936.99 K, 939.82 K, and 947.16 K.

The next figure presented, Figure 6-10, is the velocity vector for trial 5.

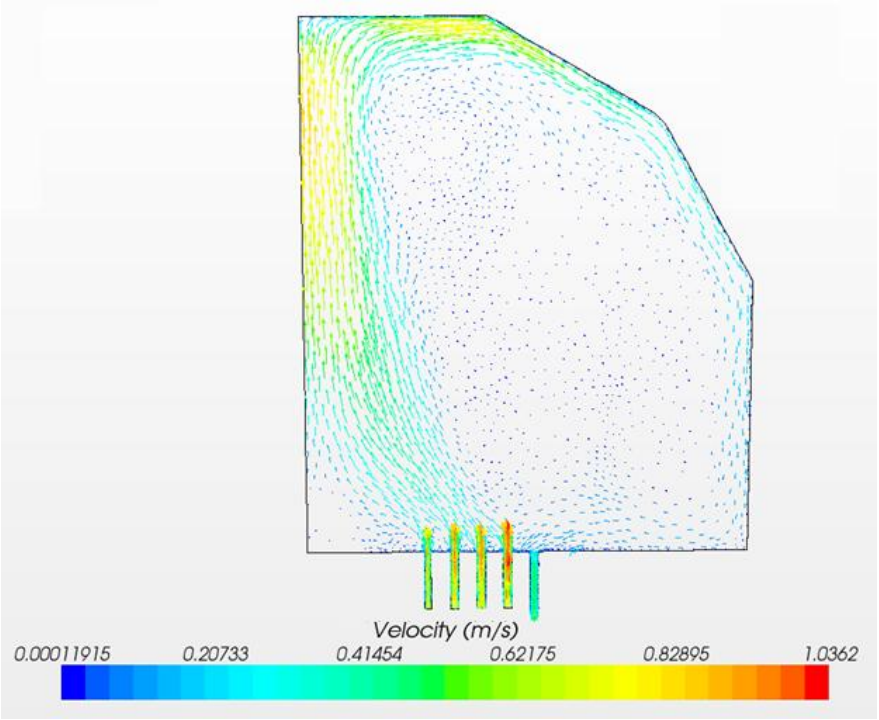

Figure 6-10: Trial 5 Velocity Vector

The gas jets in the trial 5 case exhibit the same behavior as in the trial 4 case.

The same comparisons can be drawn from the relationship between trial 2 and trial 5 as were drawn between trial 1 and trial 4. The trial 2 average temperatures are as much as 49.27 K higher than in trial 5, while the range of temperatures for trial 2 is between 11.09 and 16.64 K as compared to trial 5 which is between 49.09 K and 60.22 K. The maximum temperatures are much closer in this scenario, as they are both close to the maximum temperature in the upper plenum of 1000 K. As in previous cases, the overall temperatures in the upper plenum are lower in trial 5 than trial 2 from the increased heat transfer rate.

The next figure Figure 6-11 is the temperature profile for trial 8.

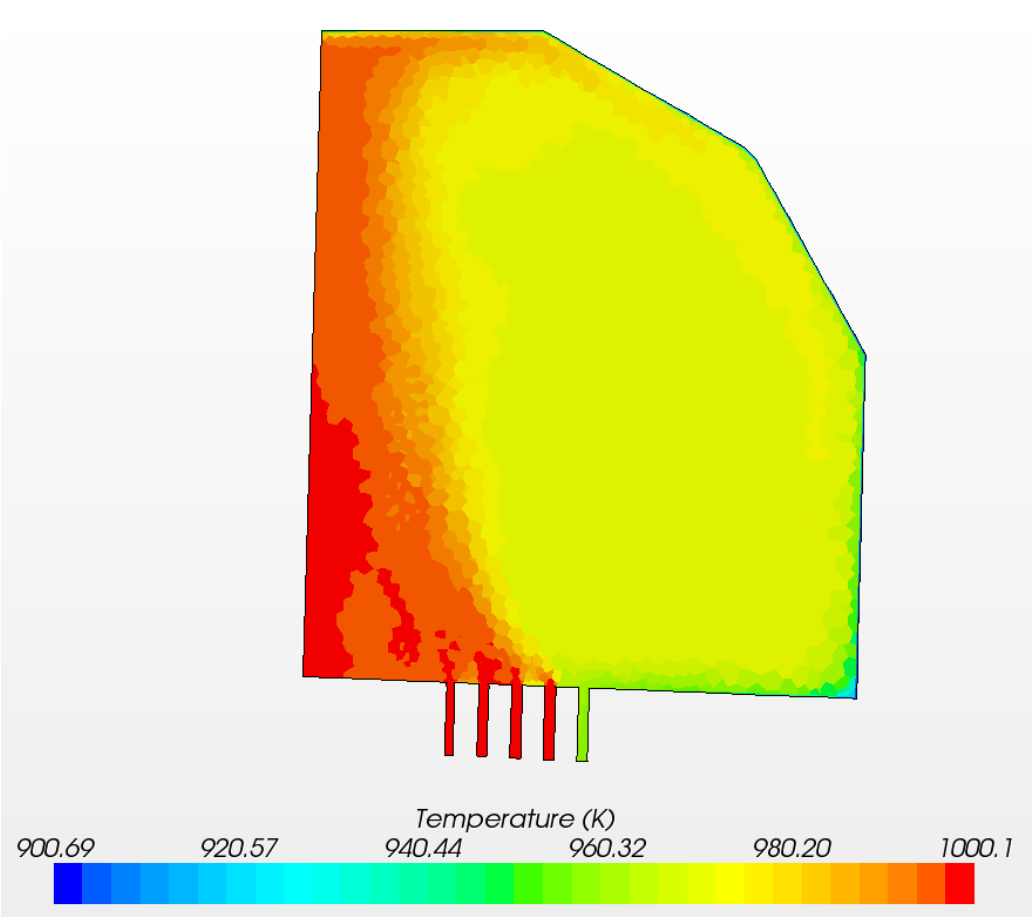

Figure 6-11: Trial 8 Temperature Profile

The same relationship exists between the trial 8 and trial 7 temperature profiles as does the trial 5 and trial 4 temperature profiles. In trial 8, the gas jets reach the upper plenum at a temperature just below 1000 K.

The maximum temperature on the three temperature planes ranges from 995.96 K at the highest temperature plane to 997.37 on the lowest temperature plane. The lowest temperature on those planes ranges from 970.53 on the lowest plane to 971.79 K on the highest plane. The average temperature on the three temperature planes from bottom to top are 942.97 K, 971.39 K, and 972.82 K.

The next figure, Figure 6-12, is the velocity vector for trial 8.

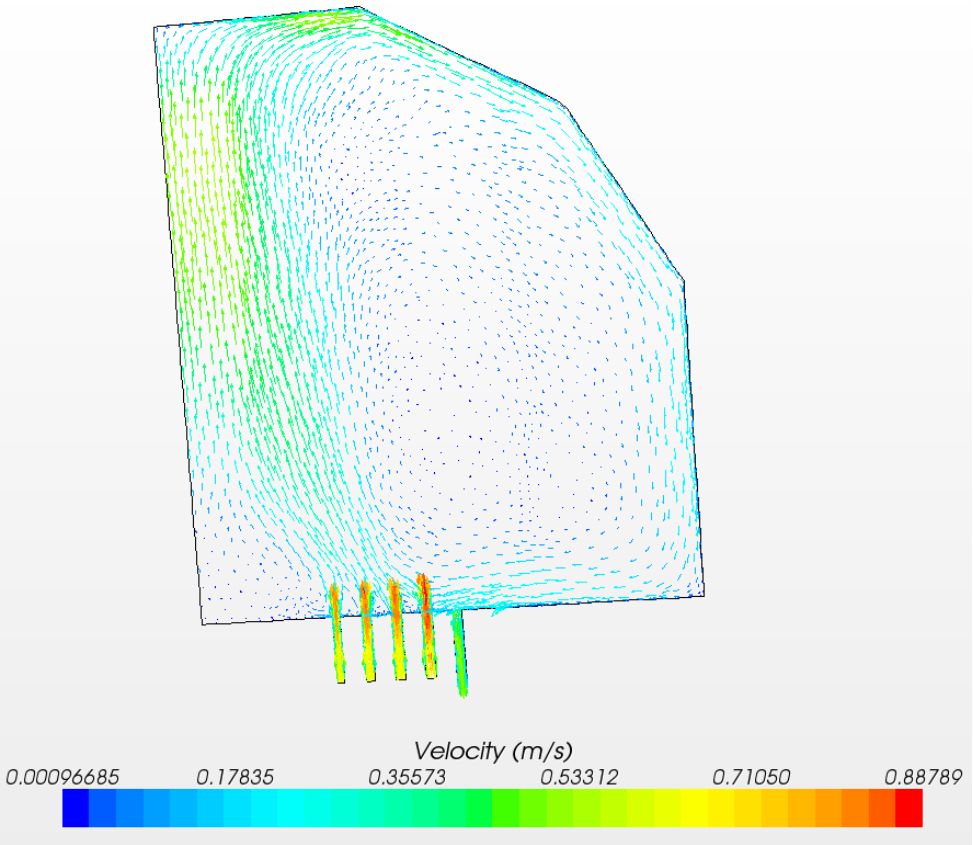

Figure 6-12: Trial 8 Velocity Vector

The gas jets in the trial 8 case exhibit the same behavior as in the trial 5 case. The two regions of differing velocities can be seen in Figure 6-11 as the 990 K region along the center of the upper plenum and the 960 K region that is directly adjacent.

The same comparisons can be drawn from the relationship between trial 2 and trial 8 as were drawn between trial 1 and trial 7. The trial 2 average temperatures are as much as 49.27 K higher than in trial 8, while the range of temperatures for trial 2 is between 11.09 and 16.64 K as compared to trial 8 which is between 49.09 K and 60.22 K. From these two it can be seen that although the gas jets reach the same point in the upper plenum in both cases, there is more mixing in the trial 2. As in previous cases, the overall temperatures in the upper plenum are lower in trial 8 than trial 2 from the increased heat transfer rate.

6.4 100% Upflow and Forced Circulation Case

Figure 6-13 shows the temperature profile for the 100% upflow case of the MHTGR.

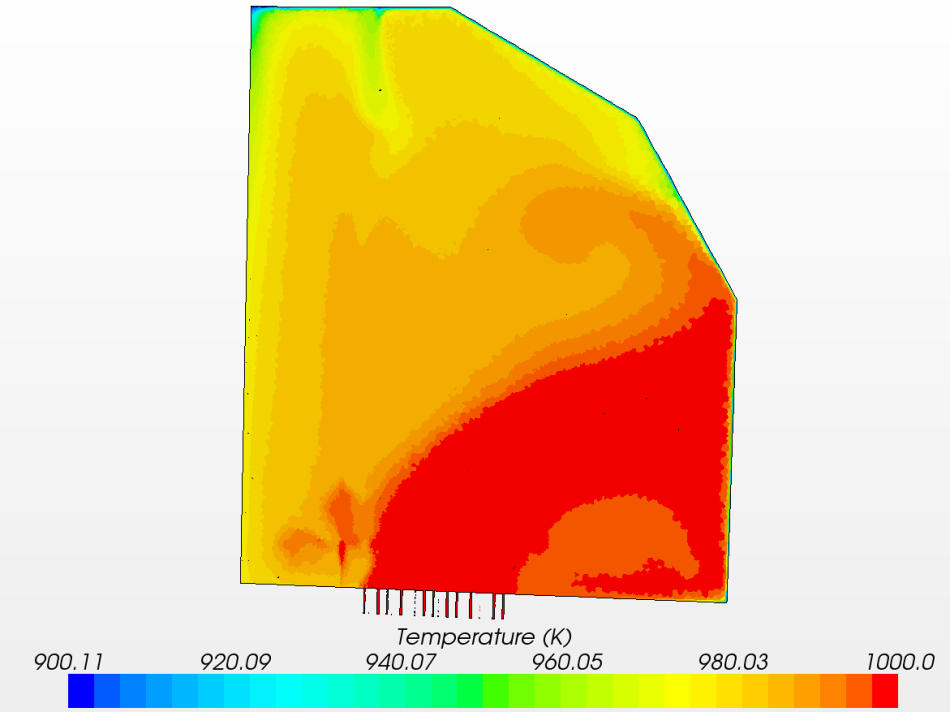

Figure 6-13: Trial 4 Temperature Profile

The gas enters through the channels closest to the center of the core at 1000K which is the inlet temperature. The core of the gas jet remains at 1000 K and come into contact with the upper plenum at along the entire lower 50% of the outer part of the upper plenum head.

The maximum temperature on the three temperature planes ranges from 984.9 K at the highest temperature plane to 999.99 K on the lowest temperature plane. The lowest temperature on those planes ranges from 981.49 K on the lowest plane to 975.30 K on the highest plane. The average temperature on the three temperature planes from bottom to top are 991.98 K, 989.00 K, and 978.76 K.

The next figure, Figure 6-14, shows the velocity vectors for trial 4.

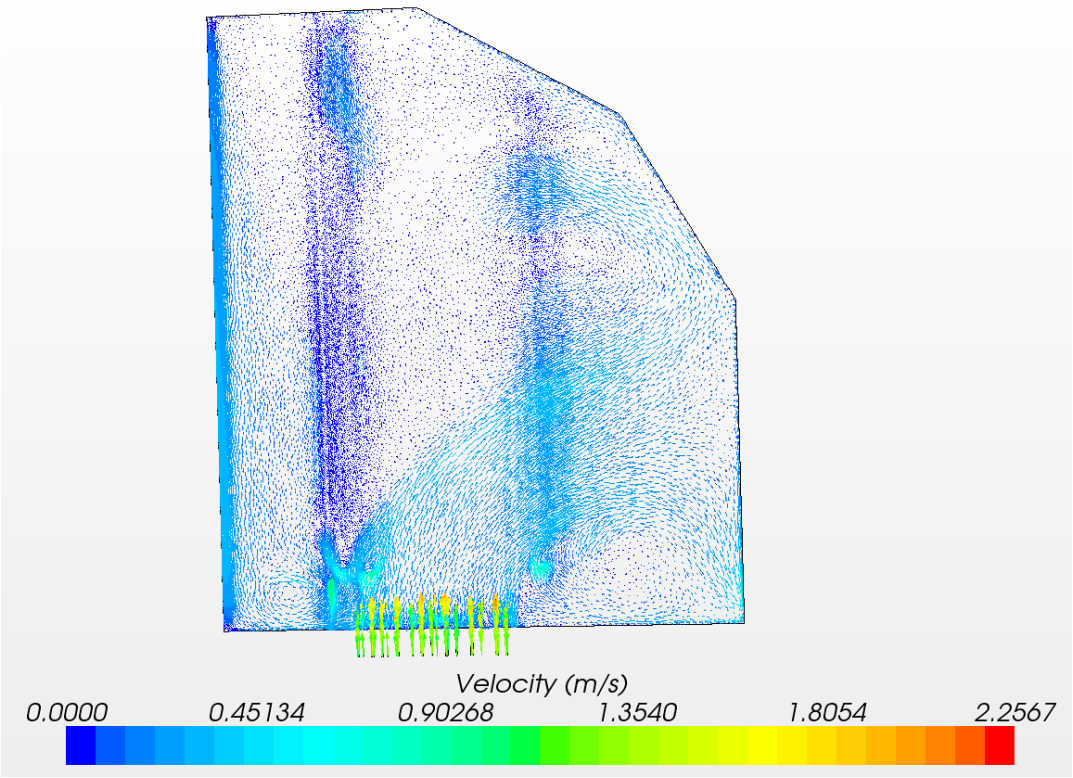

Figure 6-14: Trial 4 Velocity Vector

As seen in the thermal profile shown in Figure 6-13, the gas jets travel into the upper plenum and come into contact with the upper plenum wall at a location with the entire lower 50% of the lower plenum where some leave the upper plenum through the outlet while others are redirected along the wall and diffuse into the bulk medium of the upper plenum. Because of the change in the location of the location and orientation of outlet, there is a larger amount of communication between the outlet and the gas jet inlets resulting in a streamline between the two locations.

The next figure, Figure 6-15, shows the temperature profile for trial 6.

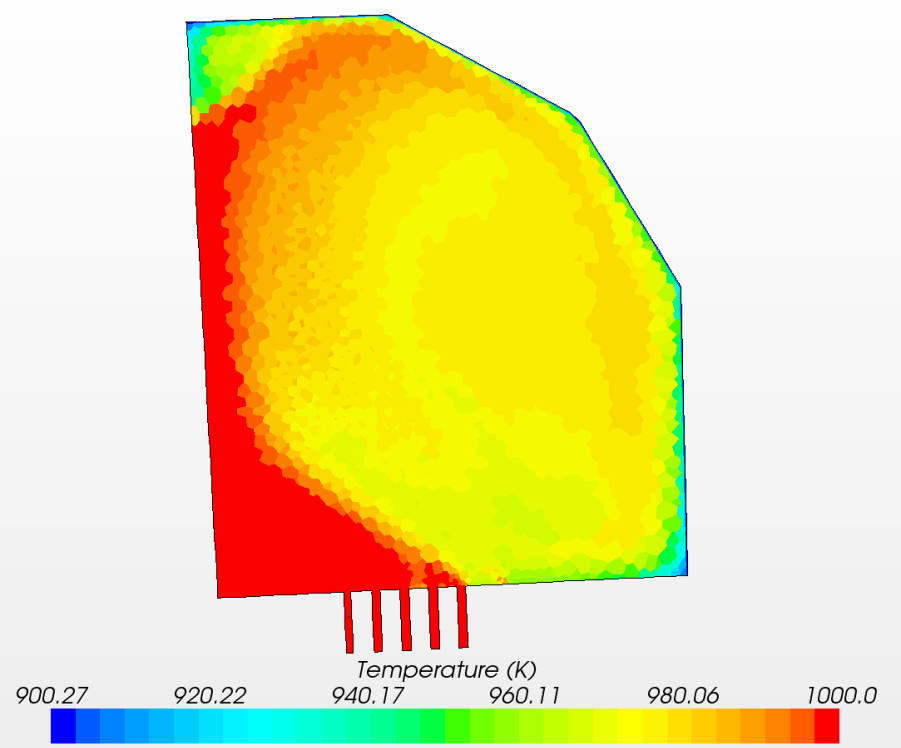

Figure 6-15: Trial 6 Temperature Profile

The gas jets enter through the upper plenum through the channels and into upper plenum at 1000 K. They lose heat as they diffuse and travel towards the center of the upper plenum and begin to mix with the overall upper plenum, until coming into contact with the top of the upper plenum at 980 K.

The maximum temperature on the three temperature planes ranges from 998.22 at the highest temperature plane to 999.99 K on the lowest temperature plane. The lowest temperature on those planes ranges from 971.12 on the lowest plane to 976.31 K on the highest plane.

The average temperature on the three temperature planes from bottom to top are 973.73 K, 974.77 K and 979.04 K.

The next figure presented, Figure 6-16, is the velocity vector for trial 6.

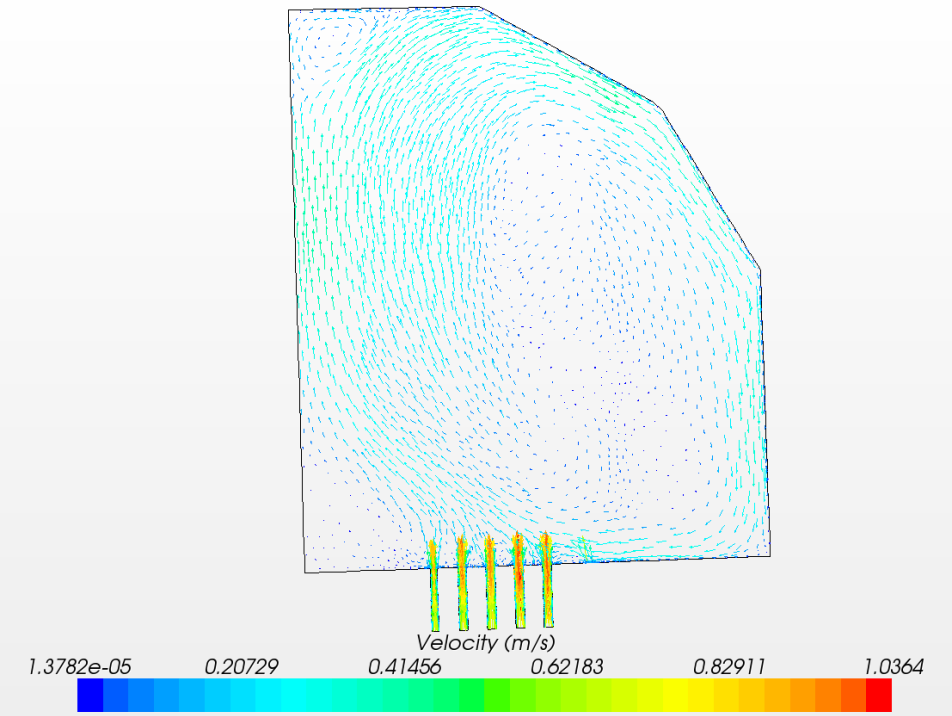

Figure 6-16: Trial 6 Velocity Vector

Upon entering the upper plenum, the gas drops to below its initial velocity as it diffuses into the upper plenum and the gas jets initially concentrate as they move towards the center of the upper plenum until the come into contact with the top of the upper plenum and redirect along the outer wall until they leave the upper plenum through the outlet channels. The same overall behavior is seen in this case as was seen in trials 4 and 5, with the major differences coming from the larger amount of flow channels. Although the gas jets do more preferentially towards the center part of the upper plenum, they do not concentrate only along the region on the between the center and the instrumentation channels but also on the outer part of the instrumentation channels as well.

The gas jets in trial 6 reach the top of the upper plenum while in trial 3 they do not. Additionally, there is more thermal mixing in the MHTGR case than in the HTTF case, and the temperature range in trial 3 is between 9.60 K and 18.50 K as compared to the

21.91 K and 28.87 K in trial 6. Additionally, the regions of higher temperature in the upper plenum are the lower regions for trial 3 while they are the higher regions for trial 6. Because the gas jets do not travel as far into the upper plenum in trial 3, they do not carry the hot gas to those upper regions like they do in trial 6.

The next figure, Figure 6-17, is the temperature profile for trial 10.

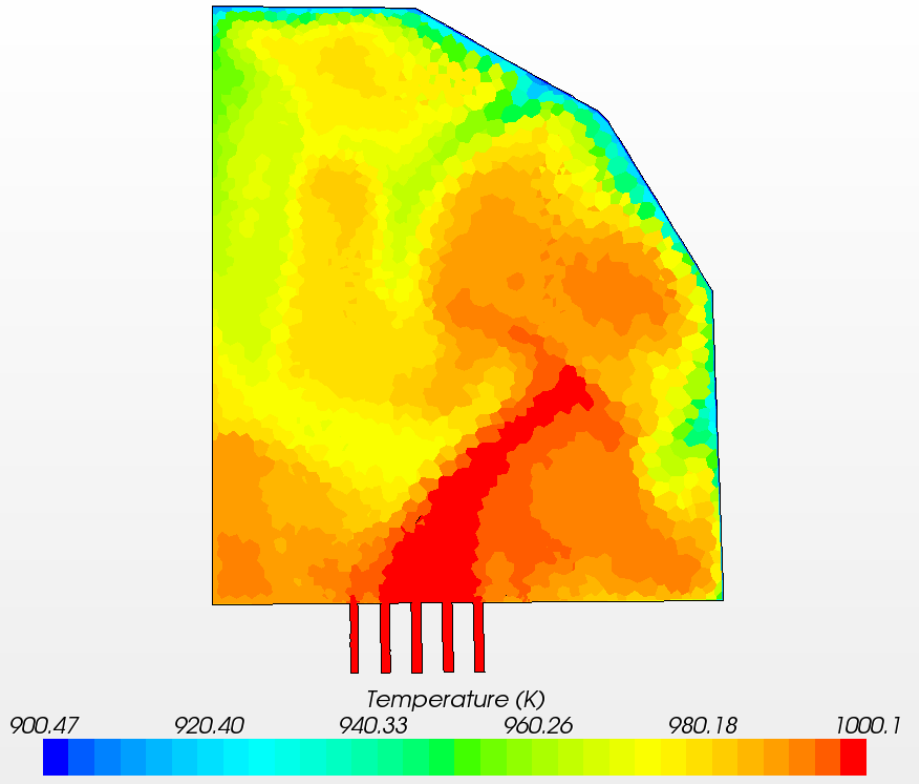

Figure 6-17: Trial 10 Temperature Profile

The gas jets enter through the upper plenum through the channels and into upper plenum at 1000 K. They move towards the outer region of the upper plenum before coming into contact with the outer part of the upper plenum wall at about 25% of the distance into the upper plenum.

The maximum temperature on the three temperature planes ranges from 998.58 at the highest temperature plane to 992.97 K on the lowest temperature plane. The lowest

temperature on those planes ranges from 951.40 on the highest plane to 972.17 K on the lowest plane.

The average temperature on the three temperature planes from bottom to top are 988.16 K, 983.09 K, and 975.63 K.

The next figure, Figure 6-18, is the velocity vectors for trial 10.

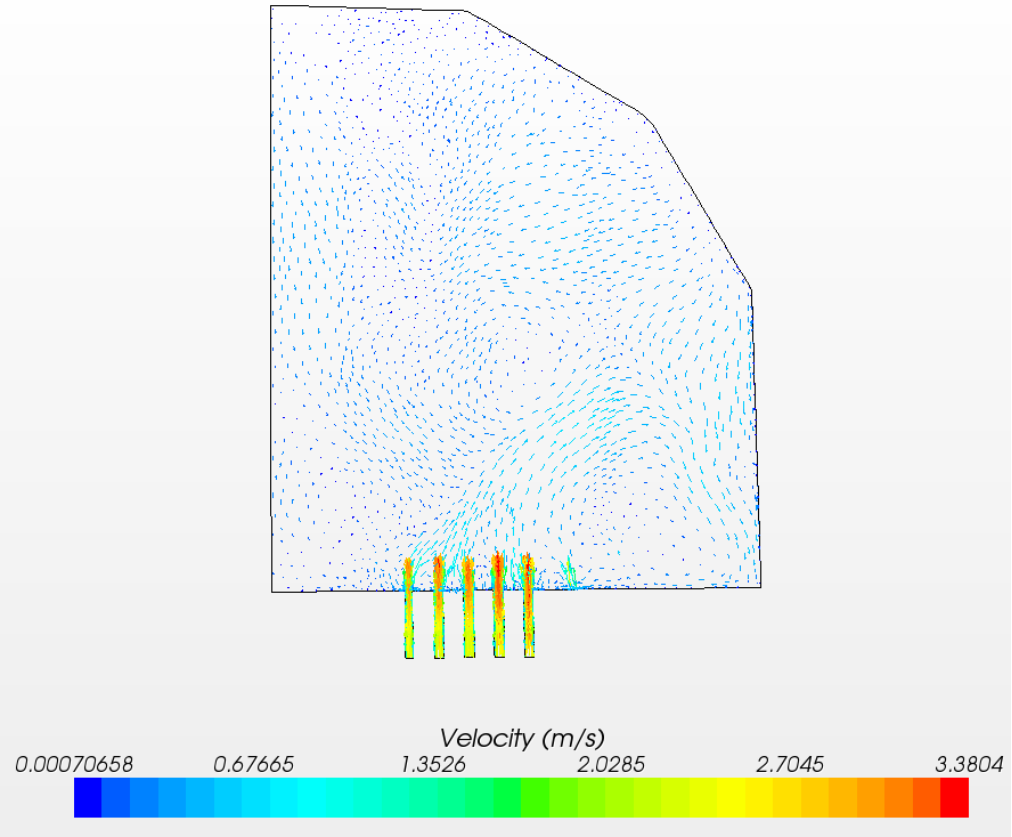

Figure 6-18: Trial 9 Velocity Vector

The gas jets enter the upper plenum and travel towards the outer region of the upper plenum before coming into contact with the upper plenum wall and leaving the upper plenum through the upper plenum inlet. Similar to the trial 3 case, the gas jets form a streamline between the flow channels and the outlet and do not travel far into the upper plenum before leaving through the outlet.

When compared to trial 3, the gas jets of trial 10 exhibit similar behavior to those of trial 3 but do not reach the same distance into the upper plenum as in trial 3. Additionally, there is more mixing in trial 3 as the temperature range is between 7.91 K and 31.97 K lower for trial 3 than for trial 10. Like in all other HTTF cases, the overall temperatures in trial 10 are lower than those in trial 3.

6.5 Results Summary and Total Comparative Analysis

A summary of the results can be seen below in Table 6-1, Table 6-2, and Table 6-3, which are the summation of results for each of the percentage upflow cases.

Table 6-1: 25% Upflow Result

Trial No.		1	4	7
Gas Jet Distance Traveled (%(		100	100	100
Temperature Plane 1 (K)	Ave.	964.4	916.72	942.97
	Max.	991.53	964.23	976.34
	Min.	962.42	915.19	942.08
Temperature Plane 2 (K)	Ave.	964.4	919.65	944.94
	Max.	990.71	963.56	975.71
	Min.	964.73	918.44	943.76
Temperature Plane 3 (K)	Ave.	967.28	925.87	949.54
	Max.	990.56	962	974.83
	Min.	965.72	923	946.89

When looking at these trials together, it can be seen while the distance the gas jets travel into the upper plenum is the same for all three cases; the temperature profiles are different. Both the HTTF simulations resulted in lower temperatures for all three regions of the upper plenum as well as higher rangers of temperatures across various planes. This shows that there is more mixing in the upper plenum for the MHTGR and that the heat transfer from the gas jets to the upper plenum head in the HTTF cases is higher. The nitrogen case, trial 7, has temperatures that are closer to the ones seen in trial 1 than trial 4 does.

Table 6-2: 50% Upflow Result

Trial No.		2	5	8
Gas Jet Distance Traveled (%)		100	100	100
Temperature Plane 1 (K)	Ave.	986.26	936.99	971.57
	Max.	999.99	994.08	997.37
	Min.	962.42	933.86	970.53
Temperature Plane 2 (K)	Ave.	965.7	939.82	971.39
	Max.	999.99	993.7	996.97
	Min.	964.73	937.03	970.65
Temperature Plane 3 (K)	Ave.	967.28	947.16	972.83
	Max.	999.99	991.9	995.96
	Min.	965.72	942.81	971.79

When looking at these trials together, the same relationships can be seen as in the 25% upflow case. Like before, the nitrogen case has temperatures that are closer to MHTGR case than the helium case does.

Table 6-3: 100% Upflow Result

Trial No.		3	6	9
Gas Jet Distance Traveled (%)		50	100	25
Temperature Plane 1 (K)	Ave.	991.98	973.73	988.16
	Max.	999.99	999.99	998.58
	Min.	981.49	971.12	972.17
Temperature Plane 2 (K)	Ave.	989	974.77	983.09
	Max.	998.99	999.99	997.38
	Min.	981.13	972.98	967.26
Temperature Plane 3 (K)	Ave.	978.76	979.04	975.63
	Max.	984.9	998.22	992.97
	Min.	975.3	976.31	951.4

When looking at these trials together, it can be seen that he natural circulation case, trial 6, and the MHTGR case, trial 3, are vastly different in both temperature profile and in the distance they travel into the upper plenum.

Trial 9 exhibits similar flow behavior as trial 3 as their gas jets turn towards the outlet channel upon entering the upper plenum but they do not go as far into the upper plenum and concentrate more towards the bottom of the outer part of the upper plenum instead of spreading across and coming into contact with the whole lower outer half of the upper plenum. Additionally both trial 9 exhibits less mixing as seen from the smaller ranges and as in all previous HTTF trials have lower overall temperatures than the MHTGR case.

The major complication to scaling this event was matching the two scaling parameters, the Reynolds number and the Froude number. In order to scale the flow area of the HTTF, the individual channel size was maintained, while the number of channels was reduced. This relationship results in a roughly four times higher L/d ratio between the two facilities which affected the ability to match both scaling parameters. As shown in chapter 4, the scaled velocity between the two facilities is a function of the length scale between the two facilities and is independent of the channel diameter which results in the Froude number being scaled well while distorting the Reynolds number. For this scenario to scale with minimal distortion in each, a gas with properties that would allow for the velocity required to match the Reynolds number parameter to be equal to the ratio calculated in chapter four of the square root of the length scale.

7 Conclusion and Future Work

7.1 Conclusion

It was the goal of this study to determine if it was possible to scale the PCC event in upper plenum of the MHTGR with respect to the HTTF through the use of CFD.

Scaling of the PCC in the upper plenum of the Modular High Temperature Gas Reactor with respect to the High Temperature Test Facility was evaluated through analytical scaling and CFD simulations. A loop momentum balance equation was used to set the velocities for the CFD simulations. Nine simulations were run as part of this work, three for the MHTGR and 6 for the HTTF: three simulations were run with 25% of the flow channels in upflow, three were run with 50% of the upflow and three simulations were run with 100% upflow. The HTTF simulations utilized two different types of gases, helium and nitrogen. Two types of HTTF simulations were run: helium or nitrogen with temperature scaling, and helium forced convection with 100% upflow when the modified Reynolds number is matched.

Of the three MHTGR simulations, two types of flow patterns exist, the gas jets reaching the center of the upper plenum, as in the 25% and 50% upflow case and the first 100% upflow case, and gas jets directing towards the outer region of the upper plenum towards the outlet like in the other 100% upflow cases. In the case of the 100% upflow case, although the gas jets in trial 9 and trial 3 both redirected towards the outlet they exhibited different behavior as the gas jet for trial 3 came into contact with the entire lower half of the outer region of the upper plenum and the trial 9 only came into contact with the lowest part. Additionally, the temperature scaled case of the HTTF using helium exhibited no characteristics of flow or thermal similarity to the MHTGR case for 100% upflow.

It has been determined that flow path similarity was preserved in the 25% and 50% upflow cases which resulted in the gas jets for both the MHTGR and the HTTF coming

into contact with the top of the upper plenum shroud; however, thermal similarity was not preserved. Due to the higher Reynolds number in the MHTGR as compared to the HTTF, more mixing occurred in the MHTGR simulations than in the HTTF simulations. Additionally, the overall average temperatures at various points in the HTTF were as much as 50 K cooler than those of the MHTGR.

The importance of this work is not to determine if or how the PCC even in the upper plenum can be perfectly matched between the HTTF and the MHTGR, but to instead determine the similarity between the two facilities and to be able to determine the difference between the two caused by the distortions. As was discussed by Ishii (25) scale distortions are inevitable in the development of an integral test facility and it is not possible to match all scaling parameters. If the distortions can be characterized, codes developed from data provided by the scaled facility can be used to model the prototype facility. In the case of this study, distortion is seen in the temperature profile in the upper plenum, which comes from the higher thermal mixing in the MHTGR and the higher surface-to-volume ratio in the HTTF. The difference in the temperature profiles that were determined in this study can be used in the further development of the HTTF. This characterization is important in the validation of the codes developed from the data provided by the HTTF. If the codes can be validated using this distortion and the data from the HTTF on the event, then it can be expected that they can be used to model the MHTGR in the upper plenum under the PCC event.

7.2 Future Work

This problem looks at the effects of the gas flowing into the upper plenum based upon thermal boundary conditions from previous studies done on gas reactors, and utilized a constant velocity based upon the average core velocity calculated. In actuality, the velocities will be highest in the hottest center regions and the velocities will decrease as they get further away from the center of the core to the cooler regions until the buoyancy of the gas is unable to overcome the gravitational forces, which is where the flow

channels will be in down flow. Additionally it is not expected that the channels are as evenly split into upflow as presented in this study and additional conditions could be looked at for more varying upflow and downflow ratios. Analyzing the overall PCC event flow patterns within the core would allow for the implementation of boundary conditions that take into account this variable radial velocity.

In addition to this, as mentioned before the HTTF has a four times larger surface area to volume ratio which results in a higher rate of heat transfer to the upper plenum head. In order to reduce the distortions caused by the difference in surface-to-volume ratio, insulation could be used on the HTTF to reduce its heat transfer rate. This could be analyzed in Star-CCM+ with the modification of the boundary condition of the upper plenum which could help to inform the use of insulation on the HTTF. As was mentioned previously, it is not possible to achieve similarity in all aspects of the PCC event in the upper plenum between the two facilities. It will be important to take into account these distortions once the tests related to this event are run on the HTTF.

Bibliography

1. Westinghouse Nuclear. *AP 1000 Brochure.* [Online] Westinghouse Nuclear, 2007. http://www.westinghousenuclear.com/docs/AP1000_brochure.pdf.

2. **MacDonald, P. E. and e. al.** *NGNP Preliminary Point Design – Results of the Initial Neutronics and Thermal-Hydraulic Assessments: INEEL/EXT-03-00870 Rev. 1.* s.l. : Idaho National Engineering and Environmental Laboratory, 2003.

3. *Advanced Power Reactors with Improved Safety Characteristics.* **Birkhofer, A.** 1995, Applied Radiation and Isotopes, Vol. 46, pp. 701-706.

4. *Decay Heat Removal in Gen IV Gas-Cooled Fast Reactors.* **Lap-Yan Cheng, Thomas Y.C. Wei.** s.l. : Hindawi Publishing Corporation, 2009, Science and Technology of Nuclear Installations.

5. *Project of the GT-MHR high-temperature helium reactor with gas turbine.* **Kiryushin, A.I. et al.** 1997, Nuclear Engineering and Design, Vol. 173, pp. 119-129.

6. *Safety Demonstration Tests on HTR-10.* **Hu, Shouyin et al.** Beijing, China : IAEA, 2004. 2nd International Topical Meeting on High Temperature Reactor Technology.

7. *Long-term high temperature operation of the HTTR.* **Goto, Minoru et al.** 2011, Nuclear Engineering and Design.

8. *Safety evaluation of HTTR.* **Kunitomi, Kazuhiko, Nakagawa, Shigeaki and Shiozawa, Shusaku.** 2004, Nuclear Engineering and Design, Vol. 233, pp. 235-249.

9. *Safety design.* **Kunitomi, Kazuhiko and Shiozawa, Shusaku.** 2004, Nuclear Engineering and Design, Vol. 233, pp. 45-58.

10. *Gas cooled fast reactor research in Europe.* **Stainbsy, Richard et al.** 2011, Nuclear Engineering and Design, Vol. 241, pp. 3481-3489.

11. *Upflow turbulent mixed convection heat transfer in vertical pipes.* **Celata, Gian Piero et al.** 1998, International Journal of Heat and Mass Transfer, Vol. 41, pp. 4037-4054.

12. *Laminar mixed convection heat transfer in a vertical circular tube under buoyancy-assisted and opposed flows.* **Mohammed, Hussein A.** 2008, Energy Conversion and Management, Vol. 49, pp. 2006-2015.

13. **Sabharwall, Piyush et al.** *CFD Analysis for Flow Behavior Characteristics During Low Flow/Low Pressure Transients for the Gas Cooled Fast Reactor.* s.l. : Idaho National Laboratory, 2007.

14. *Buoyancy-Assisted Flow Reversal in Vertical Circular Channels Within a Asymmetrically-Heated Slab.* **Cheng, Chin-Hsiang, Yu, Jiun-Huei.** 2000, International Communications in Heat and Mass Transfer, Vol. 5, pp. 645-654.

15. *Thermal Response of a Modular High Temperature Gas Reactor During Passive Cooldown Under Pressurized and Depressurized Conditions.* **H. Haque, W. Feltes, G. Brinkmann.** 236, s.l. : Nuclear Engineering and Design, 2006, pp. 475-484.

16. *Post-test analysis of helium circulator trip without scram at 3MW power level on the HTR-10.* **Chen, F. et al.** Nuclear Engineering and Design, Vol. 239, pp. 1010-1018.

17. *Heat Transport and Afterheat Removal for Gas Cooled reactors Under Accident Conditions.* Vienna : IAEA, 2000. IAEA-TECDOC-1163.

18. *Impact of Increasing MHTGR Power on Passive Heat Removal.* **TD Dunn, AA Schwartz, FA Silady.** Vienna : IAEA, 1992. IAEA-TECDOC-757: Decay Heat Removal and Heat Transfer Under Normal and Accident Conditions in Gas Cooled Reactors. pp. 83-89.

19. *Passive heat removal by vessel cooling system of HTTR during no forced cooling accidents.* **al., Kunitomi K. et.** s.l. : Nuclear Engineering and Design, 1996, Vol. 166, pp. 179-190.

20. *The design feartures of the HTR-10.* **Wu, Zongxin, Lin, Dengcai and Zhong, Daxin.** 2002, Nuclear Engineering and Design, Vol. 218, pp. 25-32.

21. *Sensitivity Studies of Modular High-Temperature Gas-Cooled Reactor Postulated Accidents.* **Ball, Syd.** 2006, Nuclear Engineering and Design, Vol. 236, pp. 454-462.

22. **Ball, S. J. and Nypaver, D. J.** *GRSAC Users Manual, ORNL/TM-13697.* Oak Ridge, TN : Oak Ridge National Laboratory, 1999.

23. *An Integrated Structure and Scaling Methodology for Sever Accident Technical Issue Resolution: Development of Methodology*. **Novak Zuber, Gary E. Wilson et al.** 1998, Nuclear Engineering and Design, Vol. 186, pp. 1-21.

24. *Scaling analysis for high temperatur GAS Reactor Test Section.* **Reyes Jr., J.N. and Groome, J.T. et al.** s.l. : Nuclear Engineering and Design, 2010, Vol. 240, pp. 397-404.

25. *The three-level scaling approach with application to the Prudue University Multi-Dimensional Integral Test Assembly (PUMA).* **Ishii, M. and Revankar., S T et al.** 1998, Nuclear Engineering and Design, Vol. 186, pp. 177-211.

26. *Heavy-gas injection in the Generation IV gas-cooled fast reactor for improved decay heat removal under depressurized conditions.* **Epiney, Aaron et al.** s.l. : Nuclear Enginering and Design, 2010, Vol. 240, pp. 3115-3125.

27. *Impingement of an impact jet onto a spherical cavity. Flor structure and heat transfer*. **Terekhov, V.I et al.** 52, 2009, Vol. International Journal of Heat and Mass Transfer.

28. *CFD-assisted scaling methodology and thermal-hyraulic experiment for a single spent fuel assembly.* **Seung Hun Yoo, Hee Cheon NO, Hyuen Min Kim, Eo Hwak Lee.** s.l. : Nuclear Engineering and Design, 2010, Vol. 240.

29. **Bechtel National, Inc., Combustion Engineering, Inc., Department of Energy, EC&G Idaho, Inc., GA Technologies, Inc., Gas-Cooled Reactor Associates, General Electric Company, Oak Ridge National Laboratory, Stone & Webster Engineering Corp.** *Preliminary Safety information Document for the Standard MHTGR: HTGR-86-024.* s.l. : Stone & Webster Engineering Corp., 1986.